Electronic Supplementary Material (ESI) for Polymer Chemistry.

Supporting information

Table of Contents

Section S1: Methods 3
Section S2: Synthesis and Characterisation of the Complexes $L^{X}Cr^{Rb}$ 4
Section S3: ROTERP and ROCOP results with CHO 12
Section S4: ROTERP results with BO 34
Section S5: Tetrapolymerisation 49
Section S6: Degradation studies 53
Section S7: Crystallography 56
Section S8: Bibliography 57

Section S1: Methods

Solvents and reagents were obtained from commercial sources and used as received unless stated otherwise. If “dried solvents” were used these were obtained by different procedures. Toluene, EtOH, n-hexane, n-pentane and CH_2Cl_2 were prepared by using an MBraun Solvent Purification System MB-SPS 800 filled with Al_2O_3. Et_2O was dried over Na/benzophenone and THF was dried over K/benzophenone under argon. d_8-THF was dried over sodium prior to vacuum transfer onto 4 Å sieves followed by three freeze pump thaw degassing cycles. NMR spectra were recorded by using a Jeol JNM-ECA 400II, Bruker Advance 600 and 700 MHz spectrometer. ^{1}H and $^{13}C\{^{1}H\}$ chemical shifts are referenced to the residual proton resonance of the deuterated solvents. CHO and BO were dried over calcium hydride at room temperature for 3 days, vacuum transferred (for CHO fractionally distilled under static vacuum) followed by three freeze pump thaw degassing cycles and stored inside an argon filled glovebox prior to use. PPNCl was recrystallized from dry CH_2Cl_2 and dried in vacuum prior to use. CO_2 Grade 5.3 (Linde) was used for all polymerization studies and dried through a VICI purifier columns prior to use. The ligands $\mathbf{L^1}H_2$, $\mathbf{L^2}H_2$, $\mathbf{L^3}H_2$, $\mathbf{L^4}H_2$, $\mathbf{L^5}H_2$ and $\mathbf{L^6}H_2$ as well as the complexes $\mathbf{L^1Cr^{Li}}$- $\mathbf{L^1Cr^{Cs}}$ were synthesised according to the literature.[1–7]

Elemental analysis was collected on a Vario EL instrument. High-resolution ESI mass spectra were obtained using a Waters UPLC-Synapt G2-S HDMS. Infrared spectra were measured using a Thermo-Nicolet Nexus 670 FTIR spectrometer with DuraSampl IR accessory in total reflection at room temperature. Differential scanning calorimetry (DSC) was measured on a Netzsch 204 F1 “Phoenix” at a heating rate of 10.0 K/min. DSC thermograms are presented for the data obtained after the first heating cycle to ensure removal of the thermal history of the sample. The molecular mass and polydispersity of the polymers were determined by a Waters 1515 Gel permeation chromatography (GPC) instrument equipped with two linear PLgel columns (Mixed-C) following a guard column and a differential refractive index detector using tetrahydrofuran as the eluent at a flow rate of 1.0 mL/min at 30 °C and a series of narrow polystyrene standards for the calibration of the columns. Each polymer sample was dissolved in HPLC-grade THF (6 mg/mL) and filtered through a 0.20 µm porous filter frit prior to analysis.

Phthalic thioanhydride (PTA) was synthesized according to an adapted literature procedure.[8] Phthalic anhydride (0.3 mol, 1.0 equiv) was dissolved in 600 mL THF and an aqueous $Na_2S{\cdot}9H_2O$ (0.2 mol, 0.7 equiv) solution was added slowly. The resulting mixture was stirred at room temperature and the reaction progress was monitored by NMR analysis. After all phthalic anhydride was consumed, THF was removed in vacuum and the aqueous phase was extracted 3 times with DCM and dried over $MgSO_4$. The crude thioanhydride was recrystallized twice from *tert*-butyl methyl ether and further purified by sublimation and stored inside a glovebox.

Section S2: Synthesis and Characterisation of the Complexes $L^{X}Cr^{Rb}$

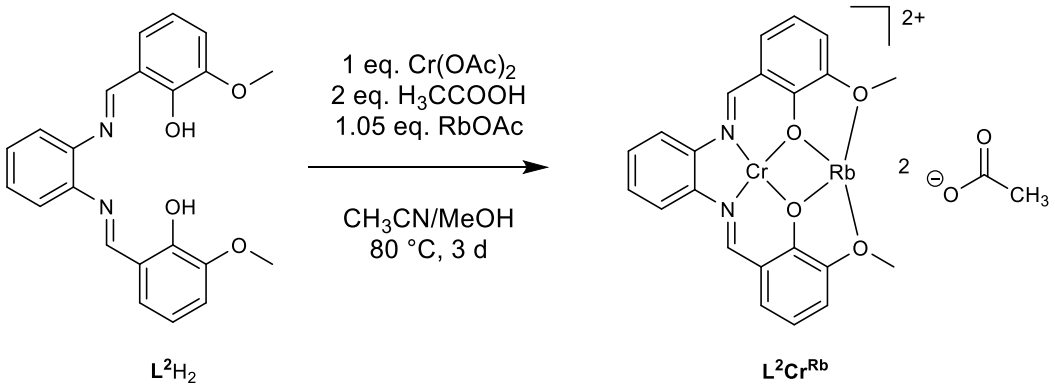

L^2H_2 L^2Cr^{Rb}

Scheme S 1: Synthesis of L^2Cr^{Rb}.

Under inert conditions L^2H_2 (1.55 g, 4.12 mmol, 1 eq.) and $Cr(OAc)_2$ (0.70 g, 4.12 mmol, 1 eq.) were dissolved in 350 mL degassed acetonitrile and stirred for 17 h at room temperature. Glacial acetic acid (2 eq.) was added, and the solution was refluxed for 7 h and then stirred for another 16 h at room temperature. The solvent was removed under reduced pressure and the crude intermediate washed three times with diethyl ether and dried to obtain a brown powder. (**L^2Cr**)

The intermediate **L^2Cr** (0.50 g, 1.03 mmol, 1 eq.) was suspended with RbOAc (0.16 g, 1.08 mmol, 1.05 eq.) in 100 mL MeOH and brought to reaction by heating briefly. The deep red solution was stirred for 16 h at room temperature. The MeOH was removed under reduced pressure and the crude product was washed three times with diethyl ether and dried to obtain **L^2Cr^{Rb}** as a brown powder. Yield: 76 %.

FTIR (L^2Cr^{Rb}): $\tilde{\nu}$ = 3404 (m, vOH, water), 3056 (w, vCH, aromatic and imine), 2963-2926 (s, vCH, methyl), 2835 (m, vCH, methoxy), 2321-1981 (w, combination and overtones, aromatic), 1718 (m, vC=O, acetate), 1606 (vs, vN=C, imine), 1540 (vs, vN-C, imine), 1434 (s, $\delta_{asym}CH_3$, methoxy), 1364-1315 (m, $\delta_{sym}CH_3$, methoxy), 1233 (s, vC-O, ether), 1190 (s, vO-Cr), 1072 (s, δCH, imine), 975 (m, vC-C, acetate), 854-651 (s-vs, δ_{oop}CH, aromatic) cm^{-1}.

ESI-MS: m/z = calculated for $[C_{22}H_{18}CrN_2O_4]^+$: 426.0667, found: 426.0712; calculated for $[C_{24}H_{21}CrN_2O_6Rb]^+$: 569.9918, found: 569.9992.

Elemental Analysis ($C_{26}H_{24}CrN_2O_8Rb$): calculated C 49.57 %, H 3.84 %, N 4.45 %; found C 49.69 %, H 3.91 %, N 4.46 %.

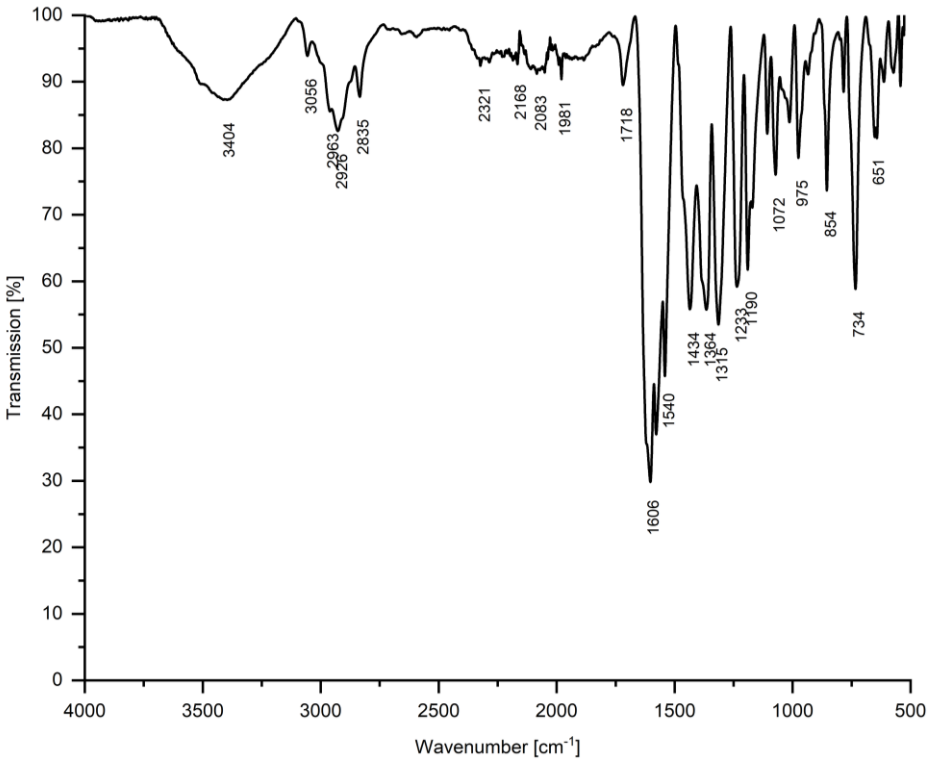

Figure S 1: FTIR Spectrum of **L^{2}Cr^{Rb}**.

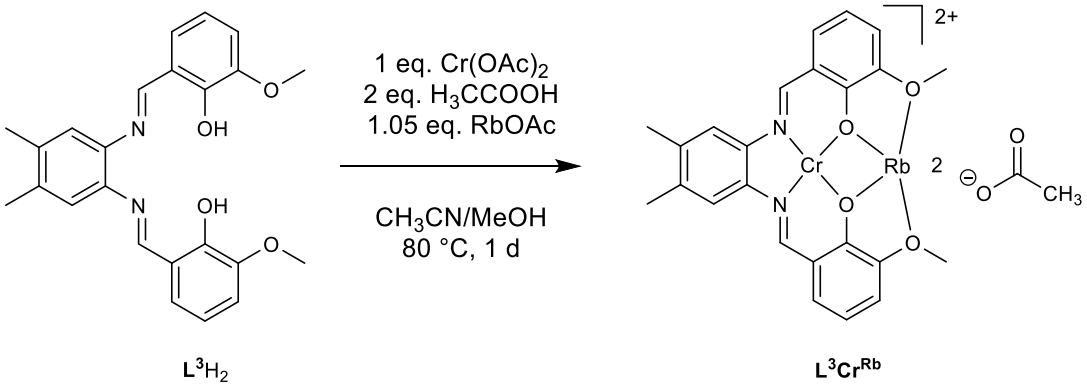

Scheme S 2: Synthesis of **L^{3}Cr^{Rb}**.

Under inert conditions **L^3**H_2 (1.58 g, 3.90 mmol, 1 eq.) and $Cr(OAc)_2$ (0.66 g, 3.90 mmol, 1 eq.) were dissolved in 350 mL degassed acetonitrile and stirred for 16 h at 80 °C. Glacial acetic acid (2 eq.) was added, and the solution was refluxed for another 3 h. The solvent was removed under reduced pressure and the crude intermediate washed five times with diethyl ether and dried to obtain a brown powder. (**L^{3}Cr**)

The intermediate **L^{3}Cr** (0.50 g, 0.92 mmol, 1 eq.) was suspended with RbOAc (0.14 g, 0.92 mmol, 1.05 eq.) in 100 mL MeOH and refluxed for 30 min. The brown suspension turned into a black solution. The MeOH was removed under reduced pressure and the

crude product was washed three times with diethyl ether and dried to obtain **L^3Cr^{Rb}** as a brown powder. Yield: 73 %.

FTIR (L^3Cr^{Rb}): $\tilde{\nu}$ = 3407 (s, vOH, water), 3058 (w, vCH, aromatic and imine), 2910 (s, vCH, methyl), 2835 (m, vCH, methoxy), 2323-1982 (w, combination and overtones, aromatic), 1717 (m, vC=O, acetate), 1618 (vs, vN=C, imine), 1550 (vs, vN-C, imine), 1473-1446 (s, $\delta_{asym}CH_3$, methoxy), 1372-1312 (m, $\delta_{sym}CH_3$, methoxy), 1222 (s, vC-O, ether), 1070 (s, δCH, imine), 855-642 (s-vs, δ_{oop}CH, aromatic) cm^{-1}.

ESI-MS: m/z = calculated for $[C_{24}H_{22}CrN_2O_4]^+$: 454.0980, found: 454.0988; calculated for $[C_{26}H_{25}CrN_2O_6Rb]^+$: 598.0231, found: 598.0234.

Elemental Analysis ($C_{25}H_{30}CrN_2O_8Rb$): calculated C 51.11 %, H 4.29 %, N 4.26 %; found C 51.15 %, H 4.33 %, N 4.29 %.

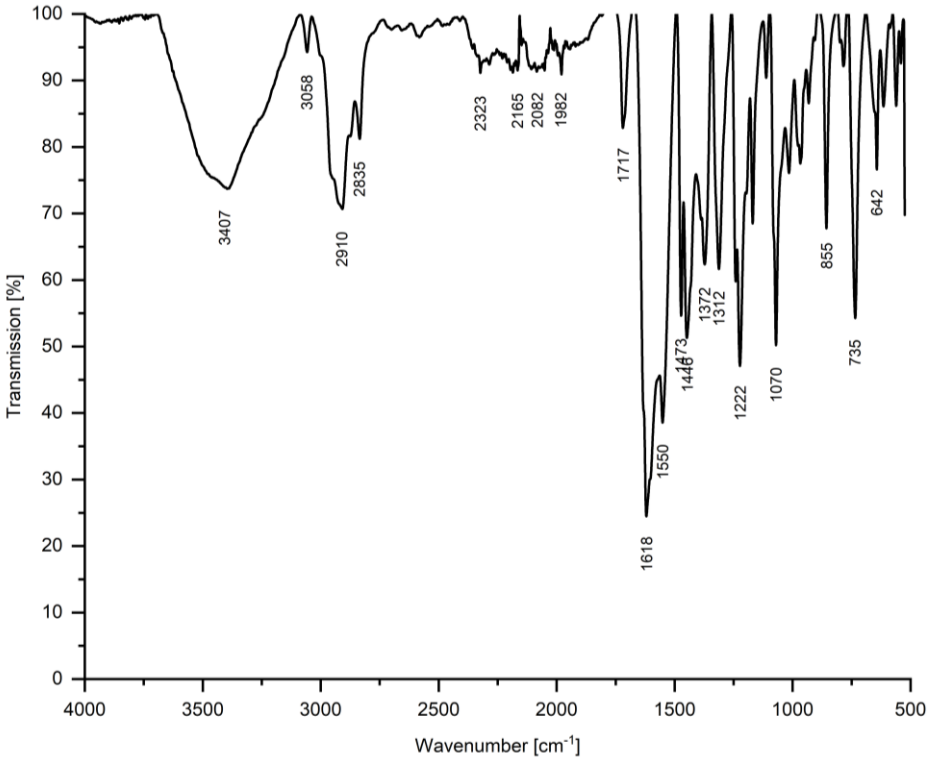

Figure S 2: FTIR Spectrum of **L^3Cr^{Rb}**.

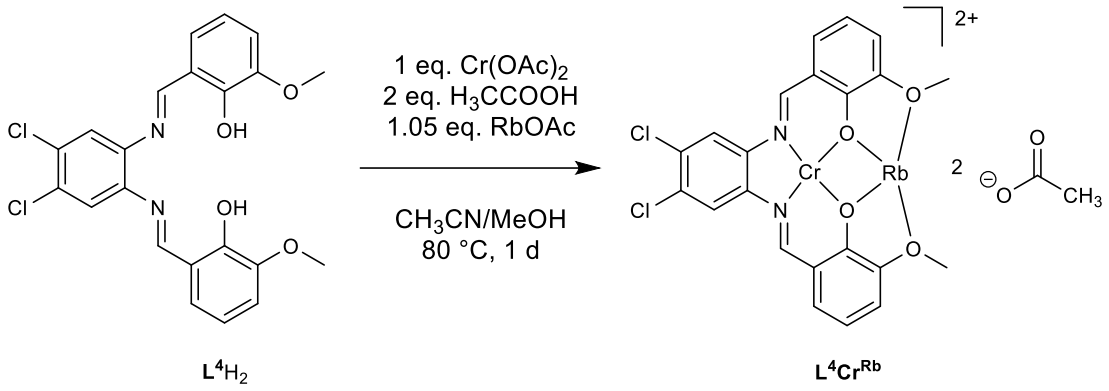

Scheme S 3: Synthesis of **L^4Cr^{Rb}**.

Under inert conditions **L^4H_2** (1.60 g, 3.61 mmol, 1 eq.) and $Cr(OAc)_2$ (0.61 g, 3.61 mmol, 1 eq.) were dissolved in 350 mL degassed acetonitrile and stirred for 16 h at 80 °C. Glacial acetic acid (2 eq.) was added, and the solution was refluxed for another 8 h. The solvent was removed under reduced pressure and the crude intermediate washed three times with diethyl ether and dried to obtain a brown powder. (**L^4Cr**)

The intermediate **L^4Cr** (0.50 g, 0.90 mmol, 1 eq.) was suspended with RbOAc (0.14 g, 0.90 mmol, 1.05 eq.) in 100 mL MeOH and brought to reaction by heating briefly. The brown suspension turned into a deep red solution. The MeOH was removed under reduced pressure and the crude product was washed three times with diethyl ether and dried to obtain **L^4Cr^{Rb}** as a brown powder. Yield: 65 %.

FTIR (L^4Cr^{Rb}): $\tilde{\nu}$ = 3424 (s, vOH, water), 3056-2963 (w, vCH, aromatic and imine), 2931 (s, vCH, methyl), 2834 (m, vCH, methoxy), 2322-1984 (w, combination and overtones, aromatic), 1705 (m, vC=O, acetate), 1601 (vs, vN=C, imine), 1540 (vs, vN-C, imine), 1432 (s, $\delta_{asym}CH_3$, methoxy), 1363 (m, $\delta_{sym}CH_3$, methoxy), 1235 (s, vC-O, ether), 1192 (s, vO-Cr), 977 (m, vC-C, acetate), 856-732 (s-vs, δ_{oop}CH, aromatic) cm^{-1}.

ESI-MS: m/z = calculated for $[C_{22}H_{16}CrN_2O_4]^+$: 493.9887, found: 493.9915; calculated for $[C_{24}H_{21}CrN_2O_6Rb]^+$: 637.9138, found: 637.9161.

Elemental Analysis ($C_{26}H_{22}Cl_2CrN_2O_8Rb \cdot 2{,}5\ H_2O$): calculated C 41.98 %, H 3.66 %, N 3.77 %; found C 41.51 %, H 3.37 %, N 3.98 %.

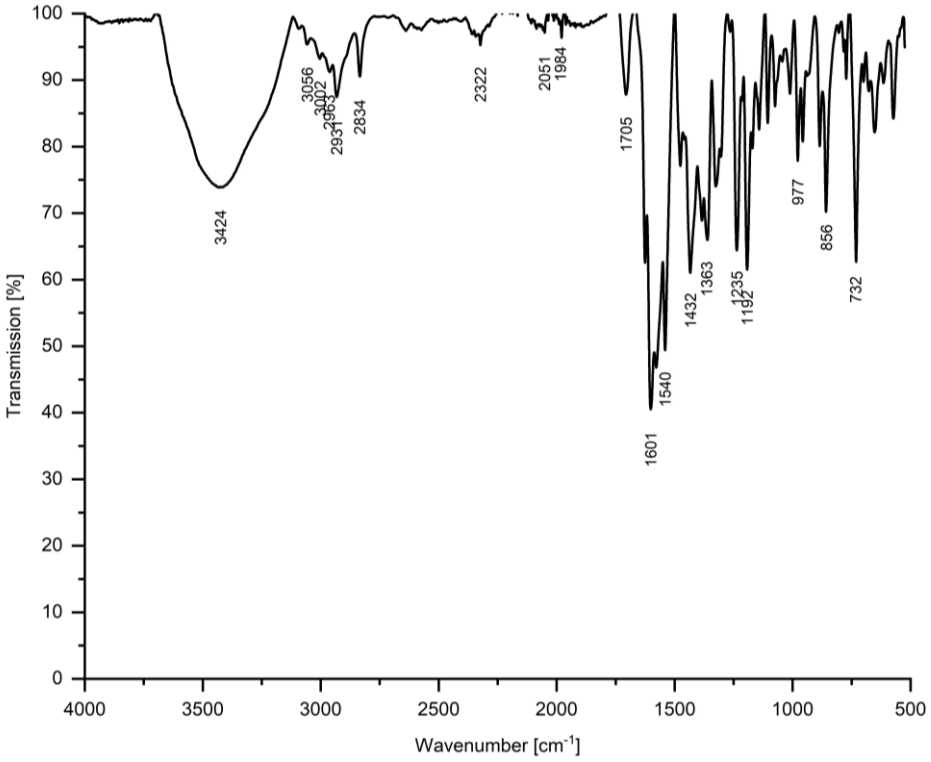

Figure S 3: FTIR Spectrum of **L^{4}Cr^{Rb}**.

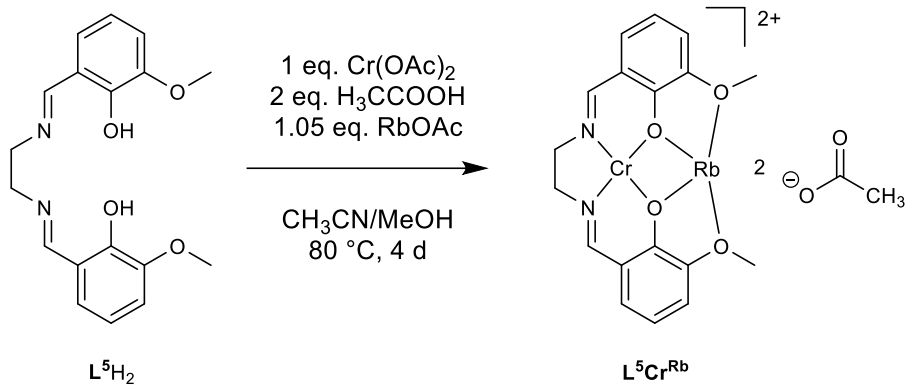

Scheme S 4: Synthesis of **L^{5}Cr^{Rb}**.

Under inert conditions **L^5**H_2 (1,50 g, 4,57 mmol, 1 eq.) and $Cr(OAc)_2$ (0,78 g, 4,57 mmol, 1 eq.) were dissolved in 350 mL degassed acetonitrile and stirred for 16 h at 80 °C. Glacial acetic acid (2 eq.) was added and the solution was allowed to react for another 72 h. The solvent was removed under reduced pressure and the crude intermediate washed three times with diethyl ether and dried to obtain a brown powder. (**L^{5}Cr**)

The intermediate **L^{5}Cr** (0.50 g, 1.14 mmol, 1 eq.) was suspended with RbOAc (0.17 g, 1.20 mmol, 1.05 eq.) in 100 mL MeOH and brought to reaction by heating briefly. The brown suspension turned into a green-brown solution. The MeOH was removed under

reduced pressure and the crude product was washed three times with diethyl ether and dried to obtain a brown powder. Yield: 91 %.

FTIR (L^5Cr^{Rb}): $\tilde{\nu}$ = 3530-3479 (s, vOH, water), 3051-2967 (w, vCH, aromatic and imine), 2918 (s, vCH, methyl), 2838 (m, vCH, methoxy), 2290-1980 (w, combination and overtones, aromatic), 1626 (vs, vC=O, acetate), 1595 (vs, vN=C, imine), 1545 (s, vN-C, imine), 1430 (s, $\delta_{asym}CH_3$, methoxy), 1374-1306 (m, $\delta_{sym}CH_3$, methoxy), 1241 (s, vC-O, ether), 1216 (s, vO-Cr), 1076 (m, δCH, imine), 859-746 (s-vs, δ_{oop}CH, aromatic) cm^{-1}.

ESI-MS: m/z = calculated for $[C_{18}H_{18}CrN_2O_4]^+$: 378.0672, found: 378.0705; calculated for $[C_{20}H_{21}CrN_2O_6Rb]^+$: 521.9923, found: 521.9902.

Elemental Analysis ($C_{22}H_{24}CrN_2O_8Rb$): calculated C 45.41 %, H 4.16 %, N 4.81 %; found C 45.72 %, H 4.16 %, N 4.87 %.

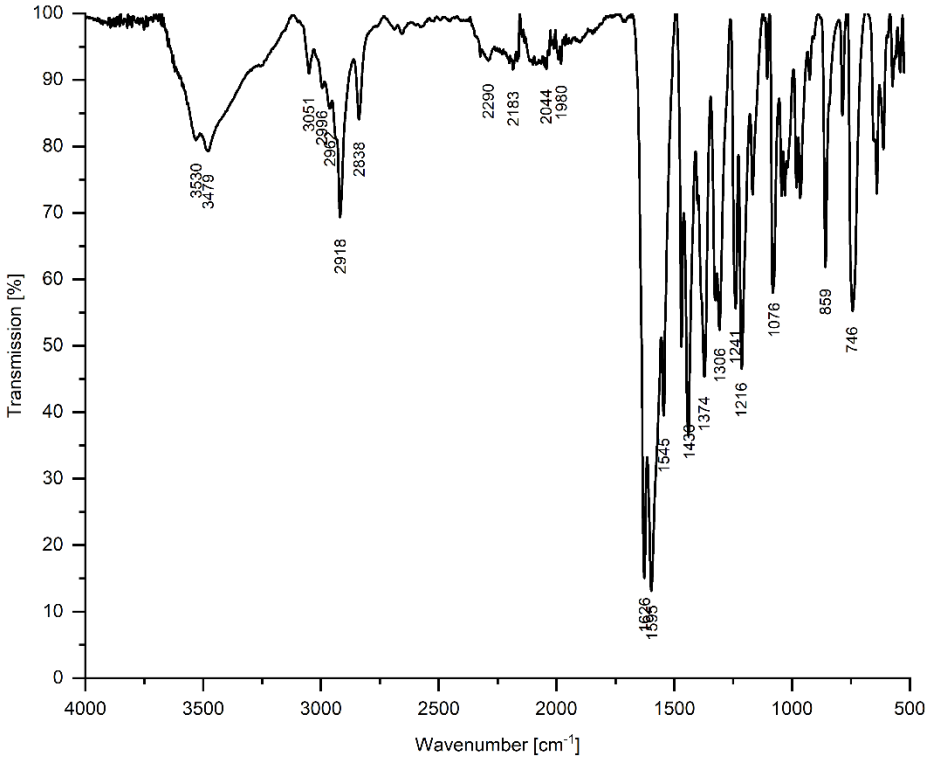

Figure S 4: FTIR Spectrum of **L^5Cr^{Rb}**.

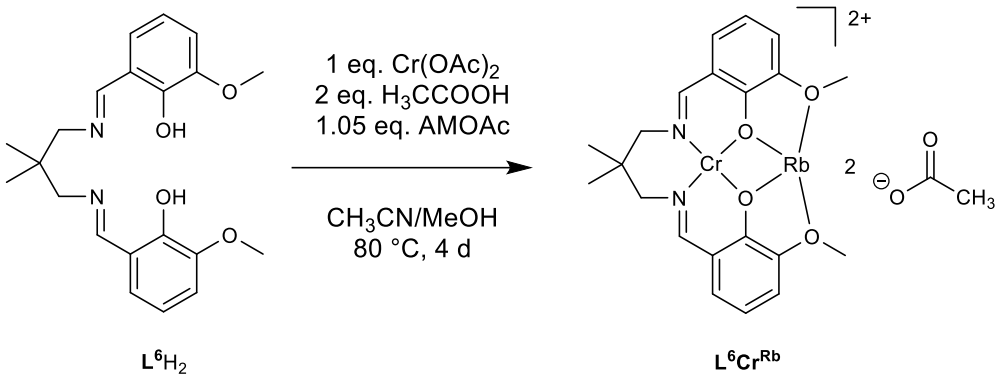

Scheme S 5: Synthesis of **L^6Cr^{Rb}**.

Under inert conditions **L^6H_2** (1.15 g, 4.13 mmol, 1 eq.) and $Cr(OAc)_2$ (0.53 g, 4.13 mmol, 1 eq.) were dissolved in 350 mL degassed acetonitrile and stirred for 17 h at 80 °C. Glacial acetic acid (2 eq.) was added and the solution was allowed to react for another 72 h. The solvent was removed under reduced pressure and the crude intermediate washed three times with diethyl ether and dried to obtain a dark green powder. (**L^6Cr**)

The intermediate **L^6Cr** (0.50 g, 1.04 mmol, 1 eq.) was suspended with RbOAc (0.16 g, 1.10 mmol, 1.05 eq.) in 100 mL MeOH and brought to reaction by heating briefly. The dark green suspension turned into a green-brown solution. The MeOH was removed under reduced pressure and the crude product was washed three times with diethyl ether and dried to obtain a brown powder. Yield: 94 %.

FTIR (L^6Cr^{Rb}): $\tilde{\nu}$ = 3059 (w, vCH, aromatic and imine), 2904 (s, vCH, methyl and methylene), 2838 (m, vCH, methoxy), 2329-1981 (vw, combination and overtones, aromatic), 1715 (m, vC=O, acetate), 1624 (vs, vN=C, imine), 1553 (s, vN-C, imine), 1446 (s, δCH_2, methylene), 1370-1313 (m, $\delta_{sym}CH_3$, methoxy), 1226 (s, vC-O, ether), 1071 (s, δCH, imine), 857-735 (s-vs, δ_{oop}CH, aromatic) cm^{-1}.

ESI-MS: m/z = calculated for $[C_{21}H_{24}CrN_2O_4]^+$: 420.1136, found: 420.1146; calculated for $[C_{23}H_{27}CrN_2O_6Rb]^+$: 564.0387, found: 564.0401.

Elemental Analysis ($C_{25}H_{30}CrN_2O_8Rb \cdot 0.5\ H_2O$): calculated C 48.12 %, H 4.85 %, N 4.49 %; found C 48.21 %, H 4.83 %, N 4.56 %.

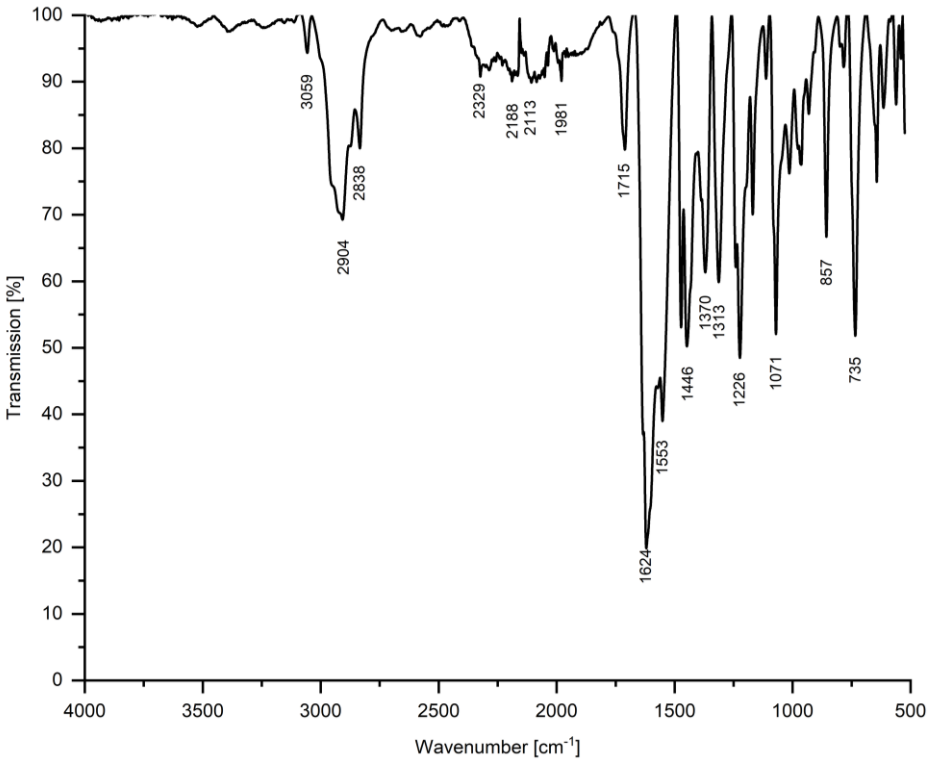

Figure S 5: FTIR spectrum of **L^6Cr^{Rb}**.

Section S3: ROTERP and ROCOP results with CHO

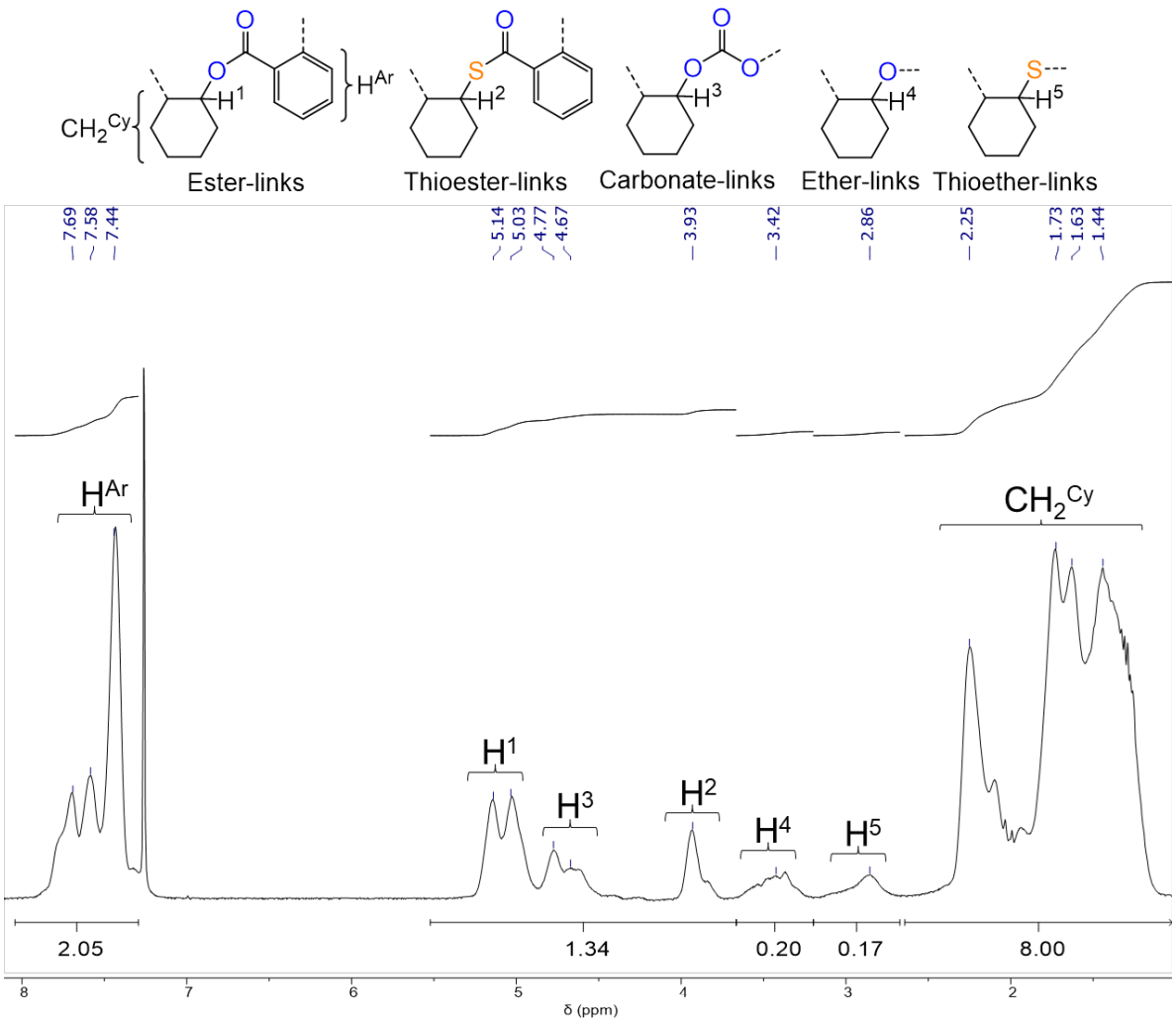

Figure S 6: ^{1}H NMR spectrum (400 MHz, $CDCl_3$, 25°C) spectrum of the precipitated terpolymer corresponding to table 1, run #7.

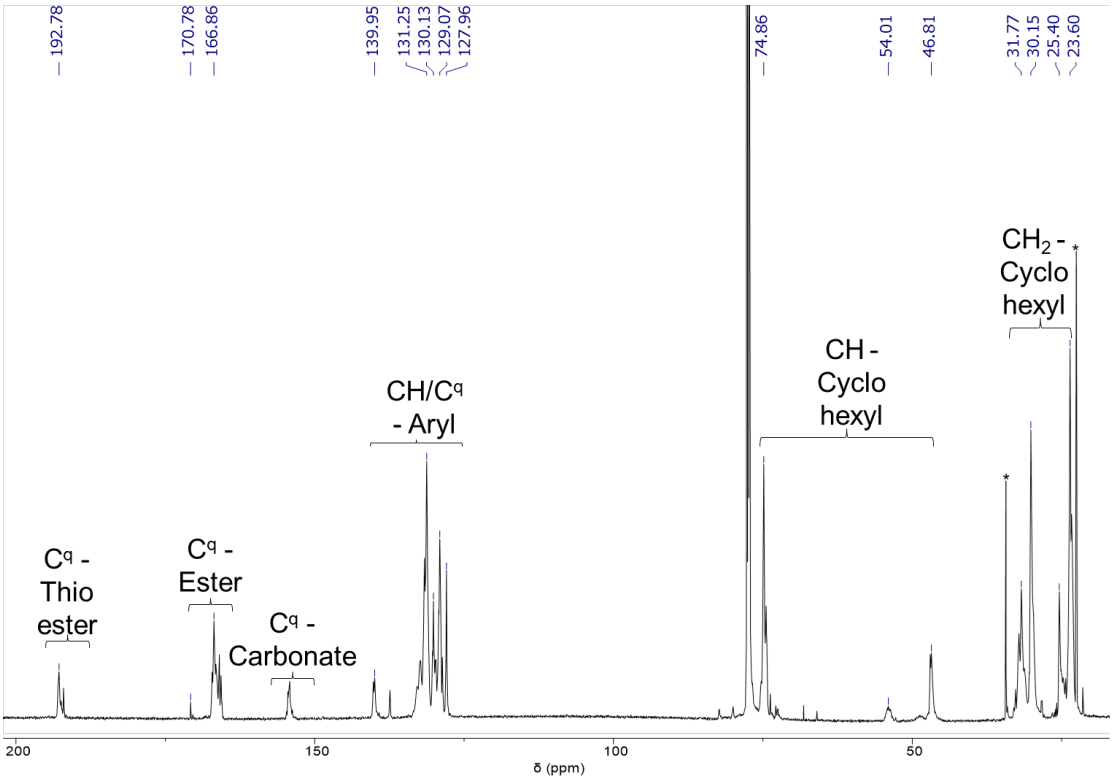

Figure S 7: ^{13}C NMR spectrum (151 MHz, $CDCl_3$, 25°C) of the precipitated terpolymer corresponding to table 1, run #7. *denotes residual pentane.

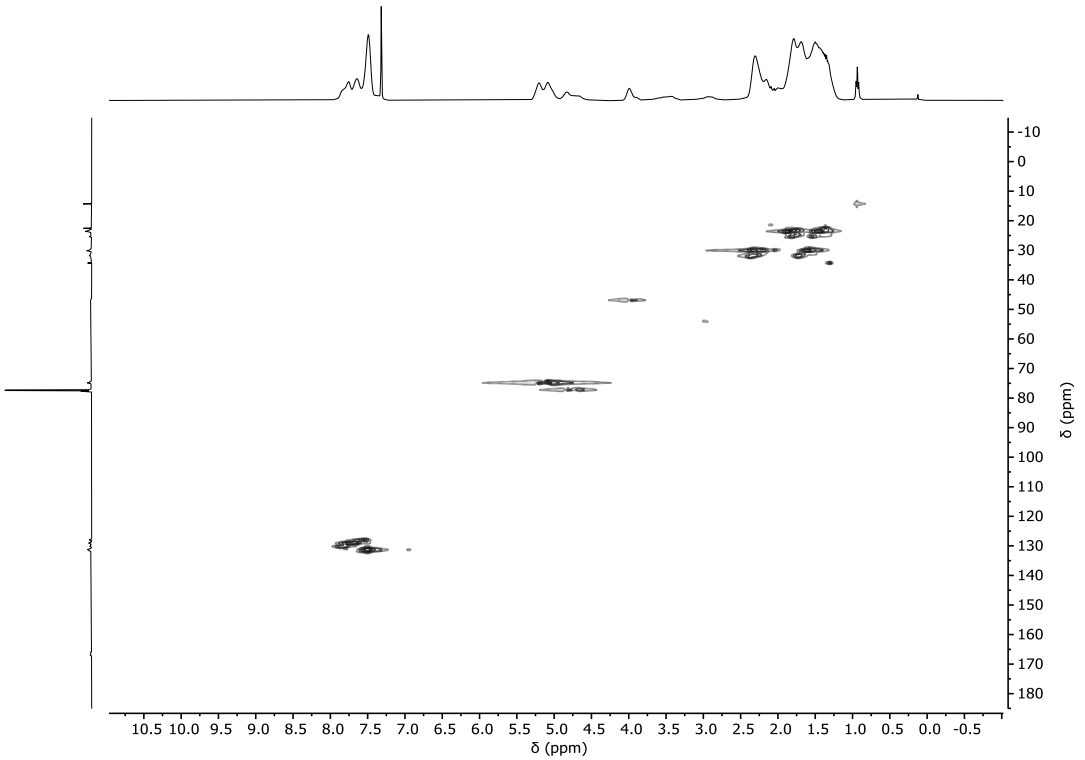

Figure S 8: ^{1}H-^{13}C HSQC NMR spectrum ($CDCl_3$, 25°C) of the precipitated terpolymer corresponding to table 1, run #7.

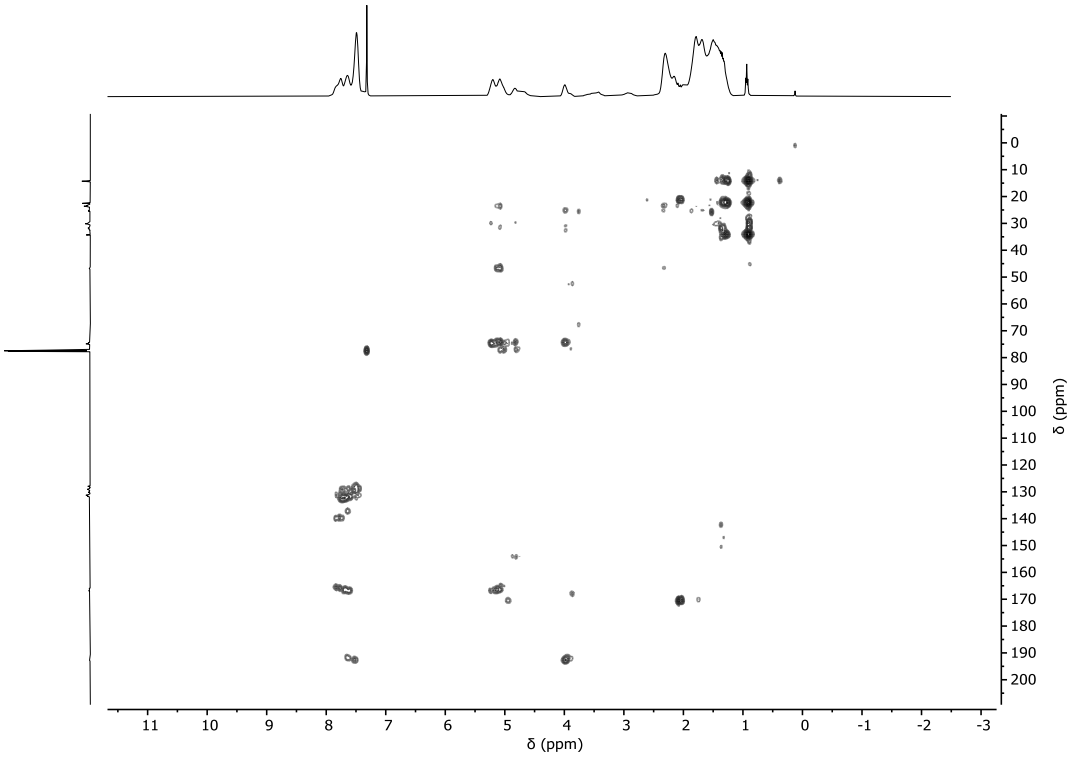

Figure S 9: ^{1}H-^{13}C HMBC NMR spectrum ($CDCl_3$, 25°C) of the precipitated terpolymer corresponding to table 1, run #7.

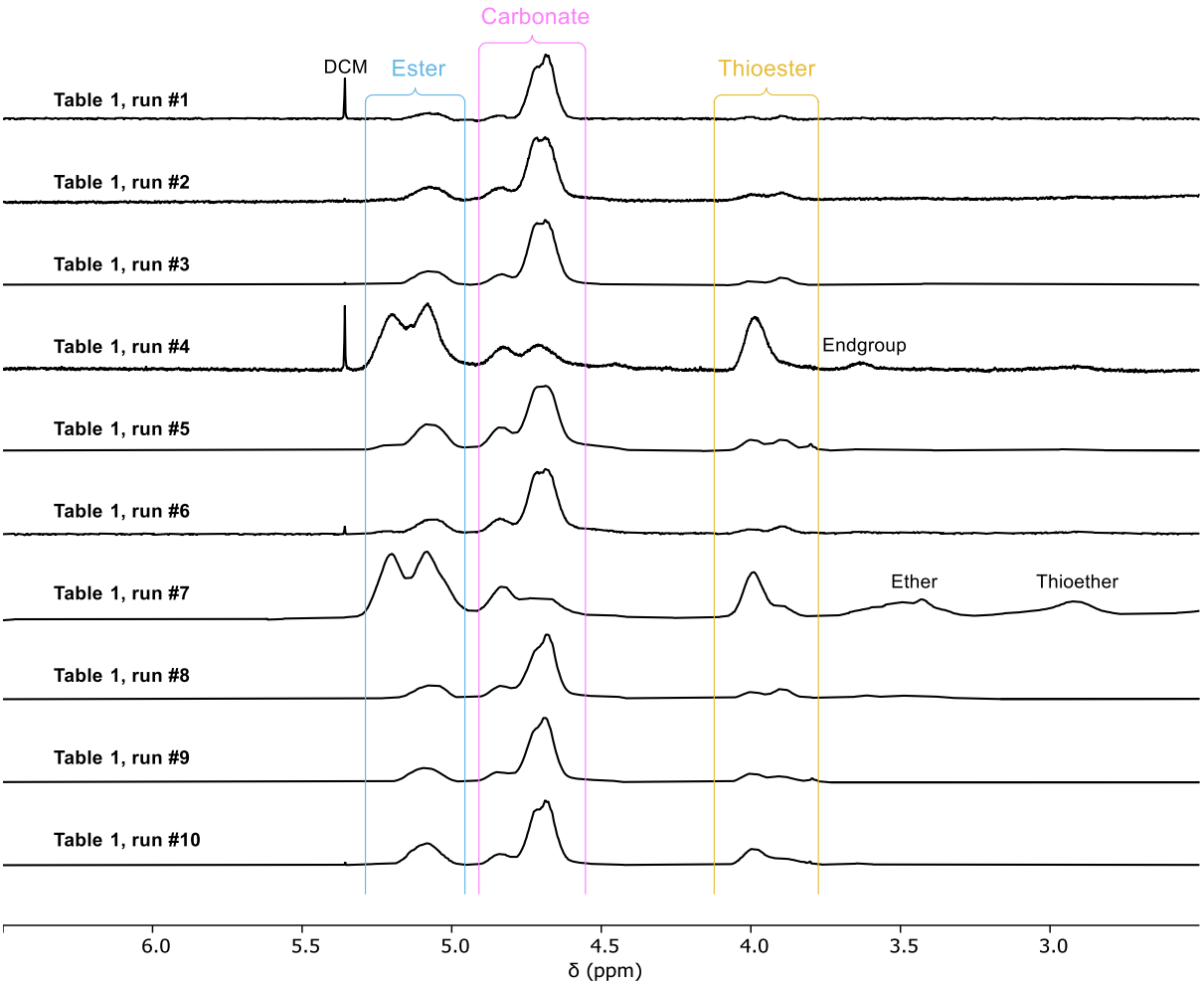

Figure S 10: Zoom into the tertiary CH region adjacent to the carbonate, ester and thioester groups corresponding to table 1 run #1-10.

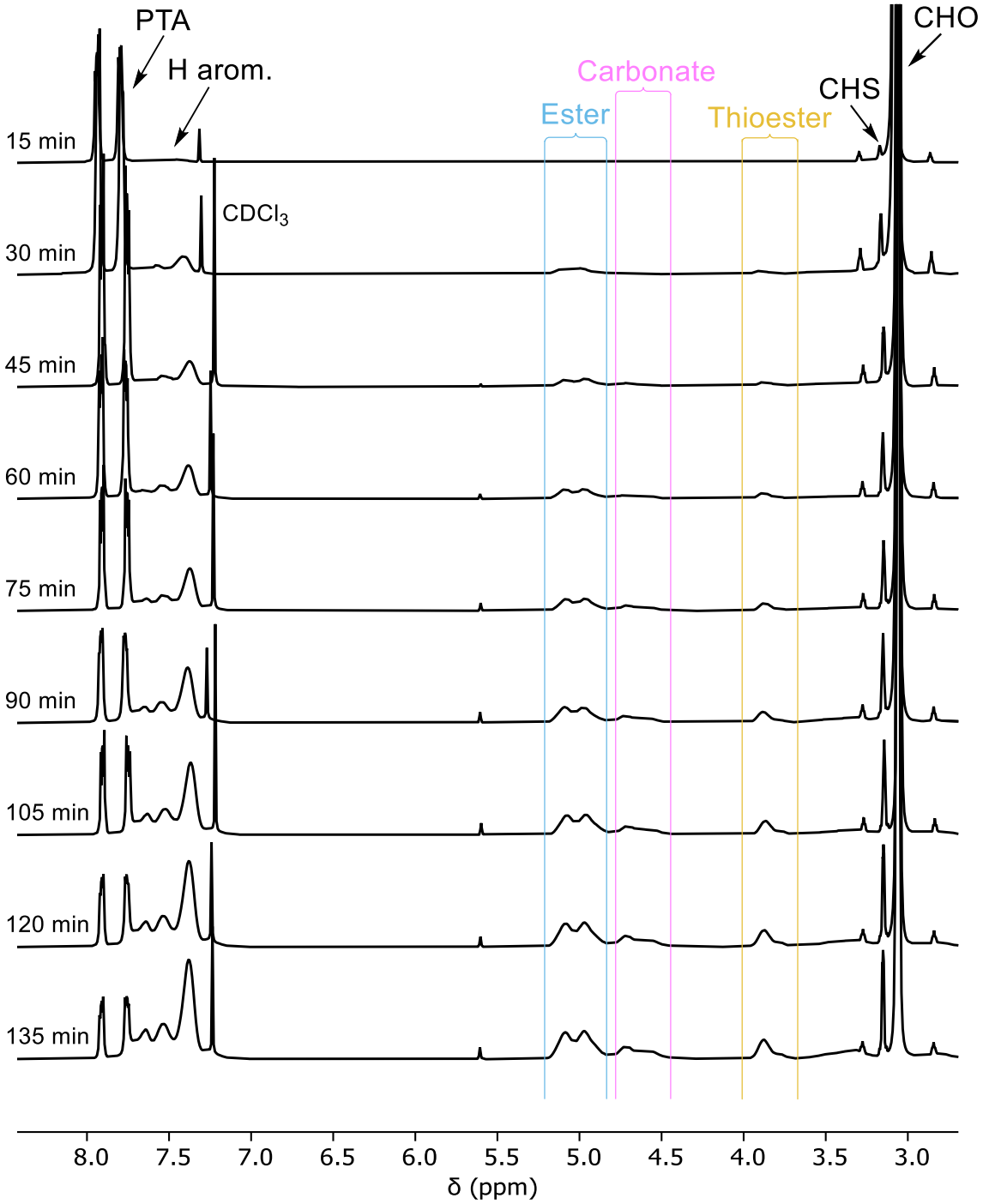

Figure S 11: Overlaid ^{1}H NMR spectra (400 MHz, $CDCl_3$, 25°C) of the aliquots taken during terpolymerisation corresponding to table 1, run #7. The plot shows the consumption of PTA and CHO, while the signals of the aromatic H atoms in the polymer repeat unit and the signals indicating the ester, carbonate and thioester links as well as the signal for cyclohexene sulfide (CHS) increase steadily.

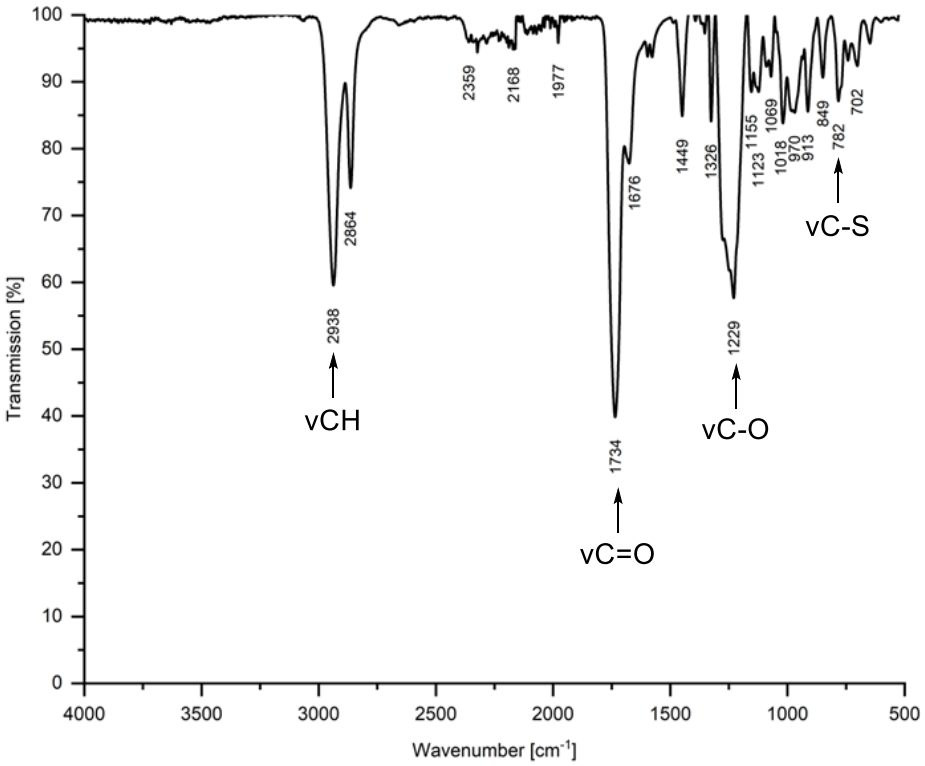

Figure S 12: FTIR spectrum of the precipitated terpolymer corresponding to table 1, run #2.

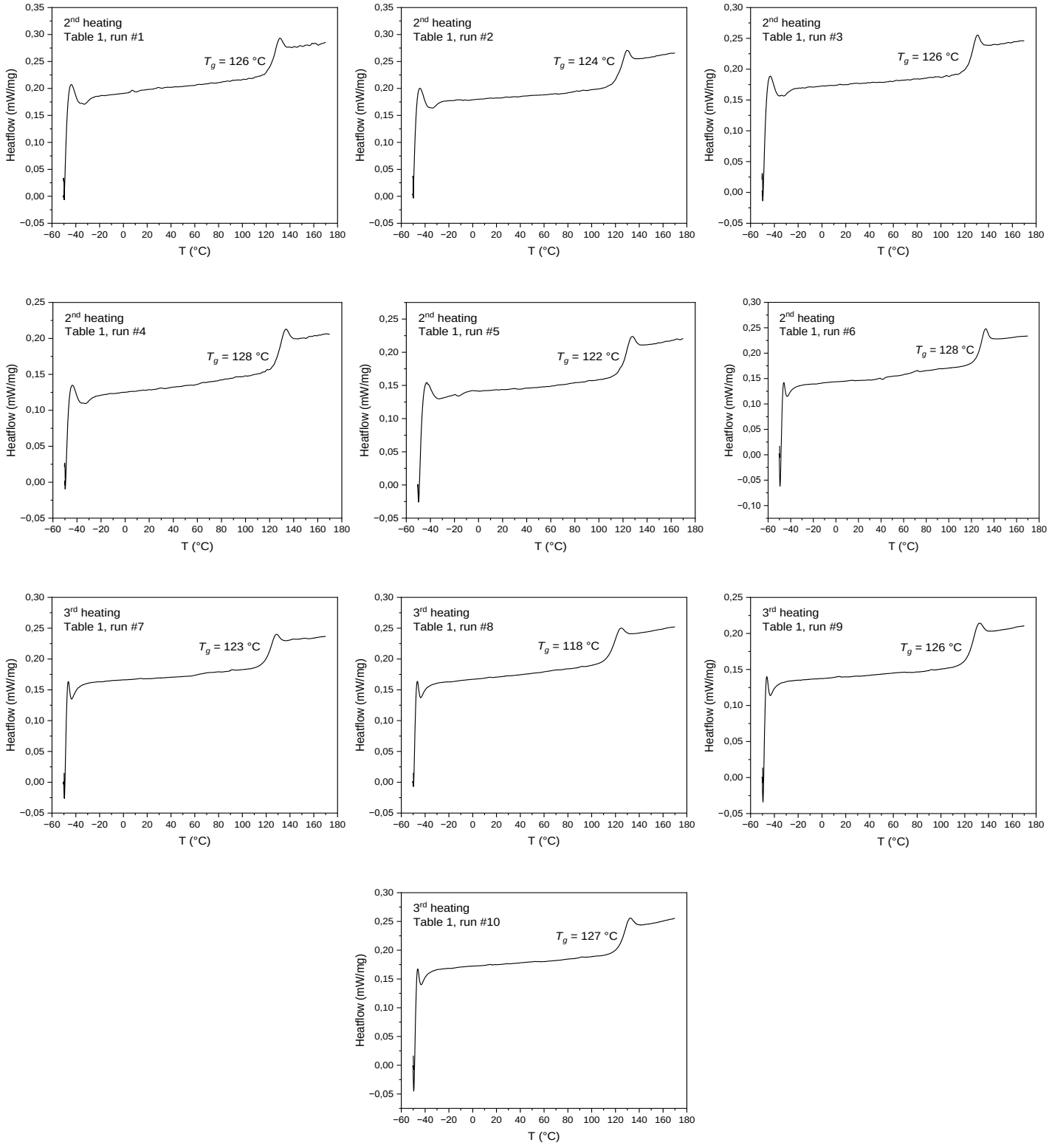

Figure S 13: DSC heating curves of the polymer corresponding to table 1, run #1-10.

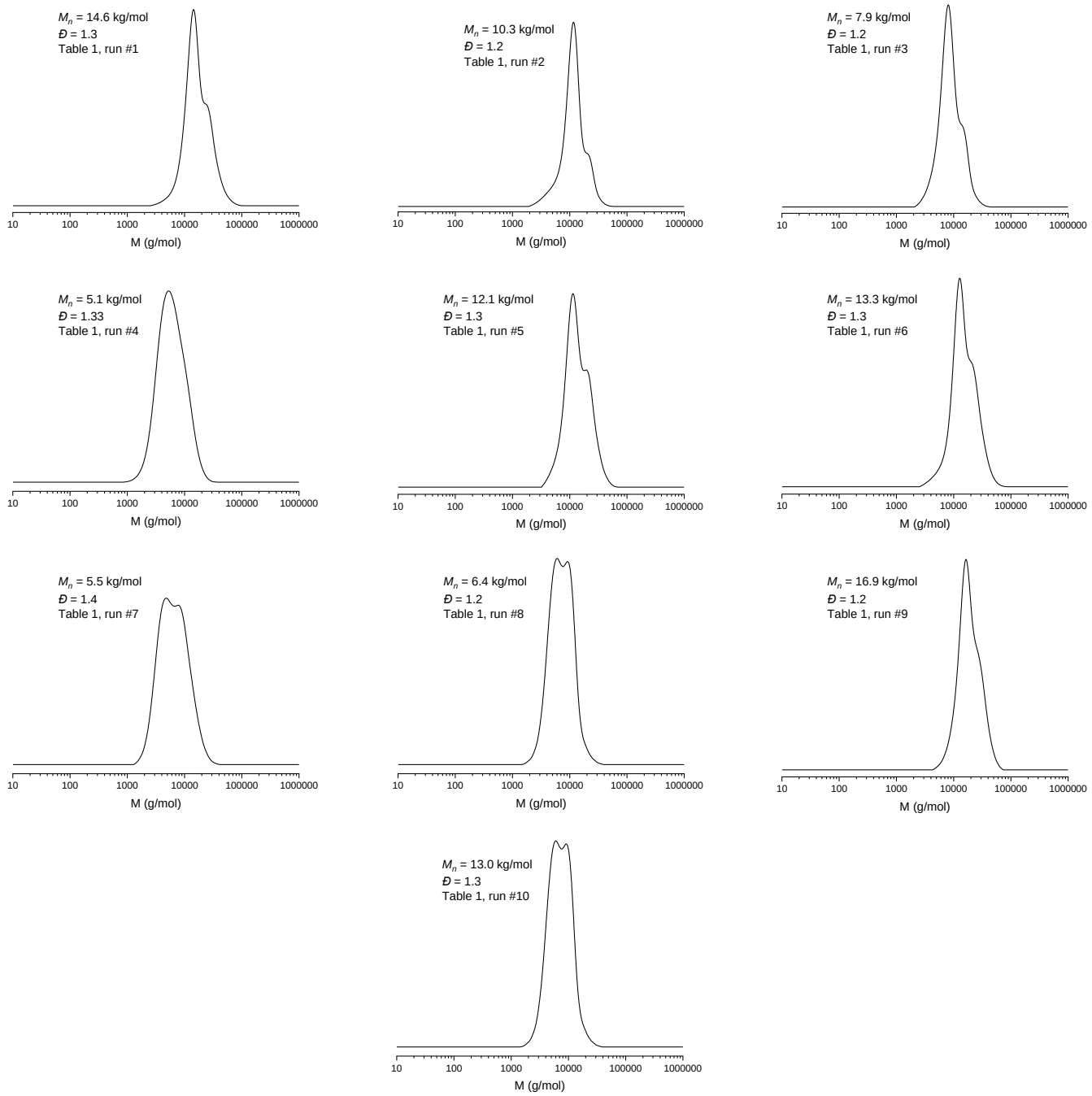

Figure S 14: GPC trace corresponding to table 1, run #1-10.

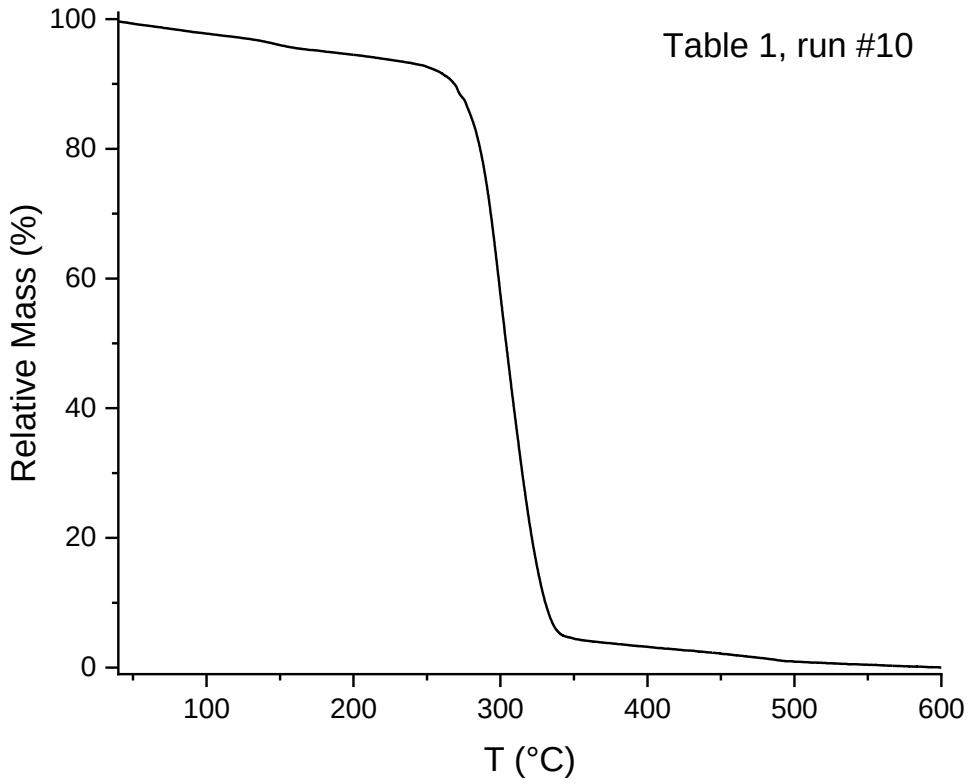

Figure S 15: TGA data of the polymer corresponding to table 1, run #10.

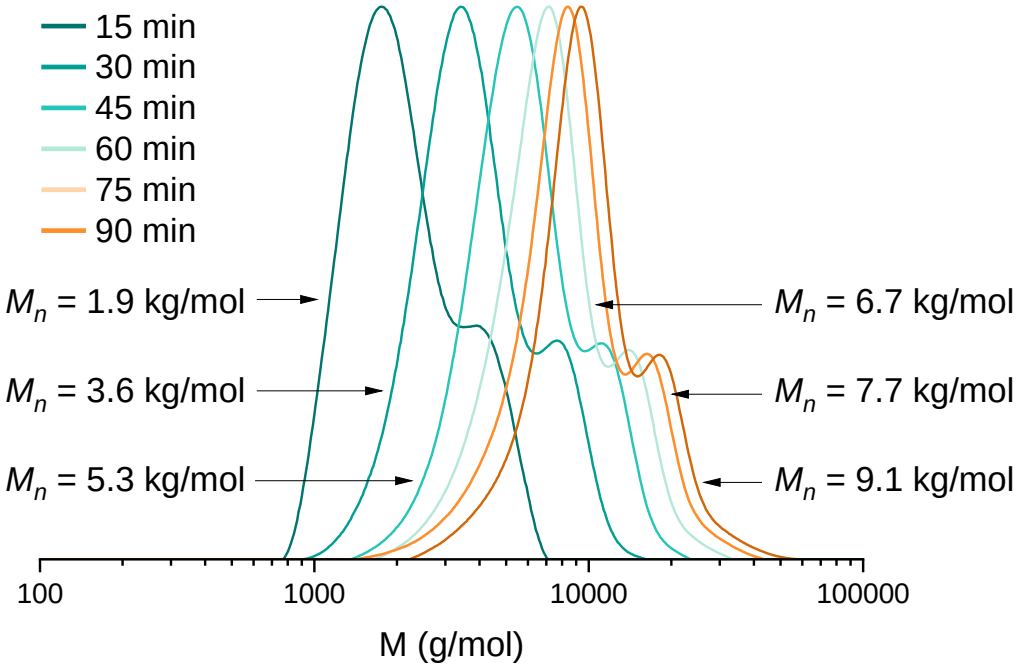

Figure S 16: GPC trace of the aliquots taken from table 1, run #1. The plot shows linearly increasing molecular weights with reaction progress.

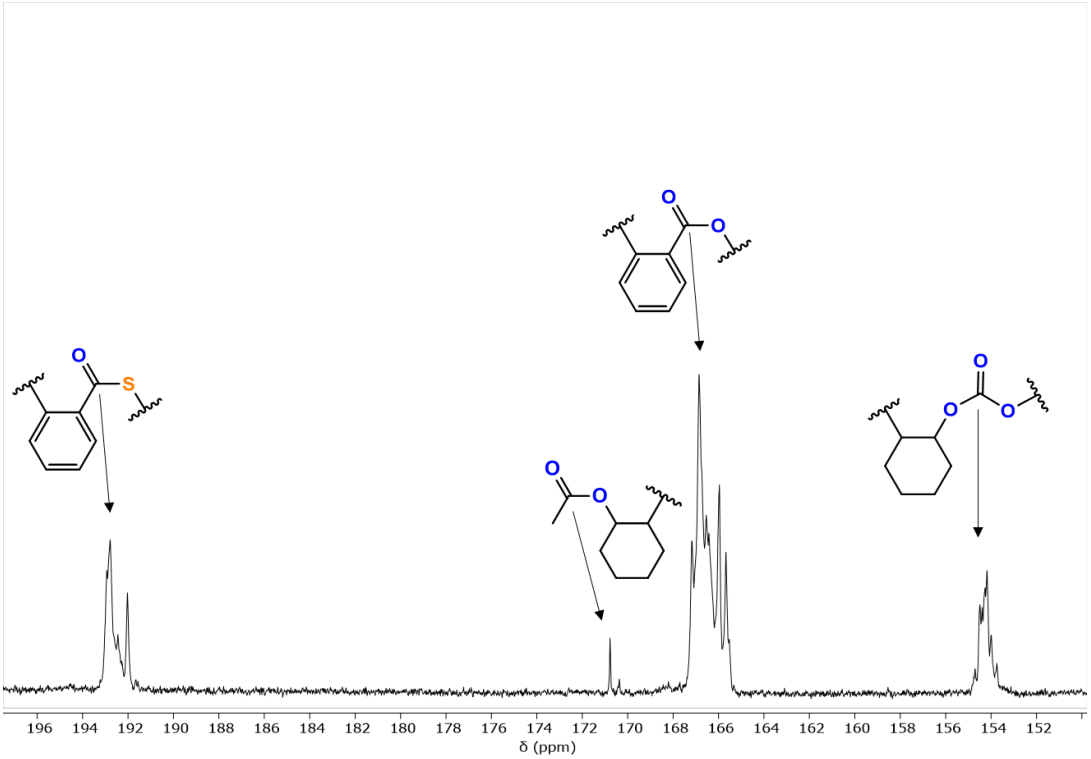

Figure S 17: Zoom into ^{13}C NMR spectrum (151 MHz, $CDCl_3$, 25°C) of the precipitated terpolymer corresponding to table 1, run #7 showing aliphatic esters resulting from acetate initiation.

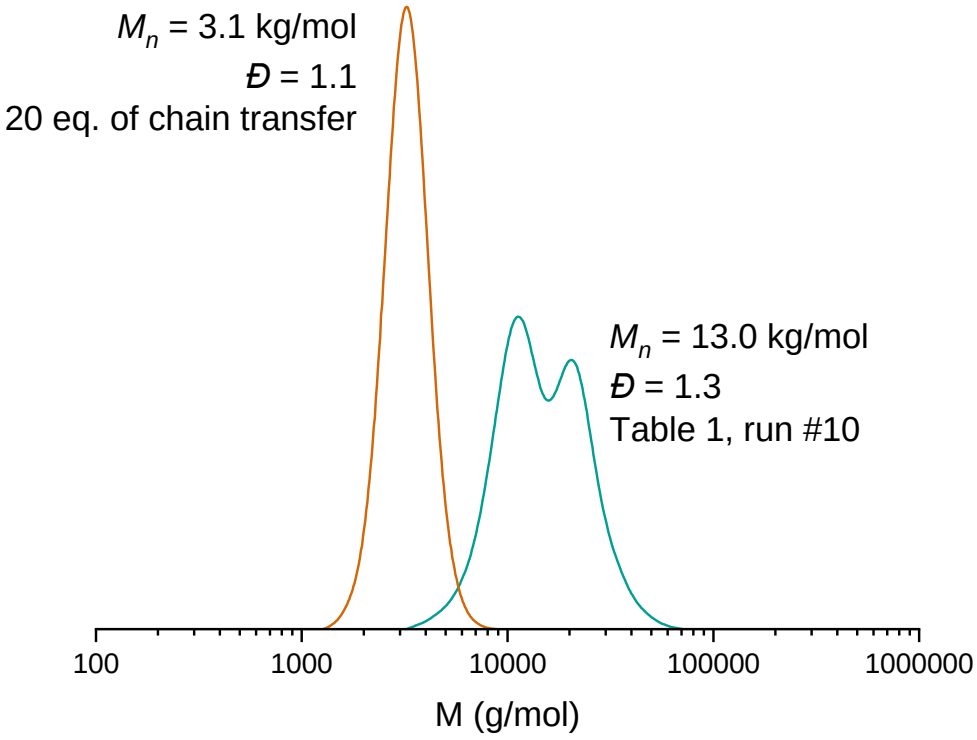

Figure S 18: GPC traces of the terpolymer corresponding to table 1, run #10 with and without the addition of 20 equiv. 1,4-Benzendimethanol acting as a chain transfer agent showing a clear decrease of the obtained M_n and a narrowed monomodal distribution in the latter case.

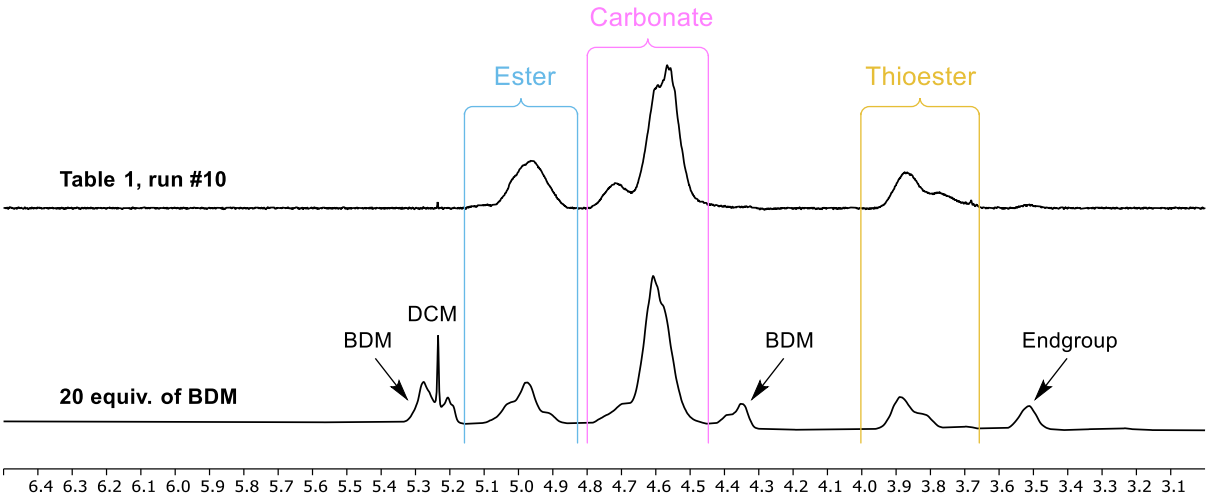

Figure S 19: Zoom into ^{1}H NMR spectrum (400 MHz, 25°C, $CDCl_3$) of the terpolymer corresponding table 1, run #10 with and without the addition of 20 equiv. 1,4-Benzendimethanol acting as a chain transfer agent showing that BDM has been incorporated into the polymer structure without effecting the linkage ratio.

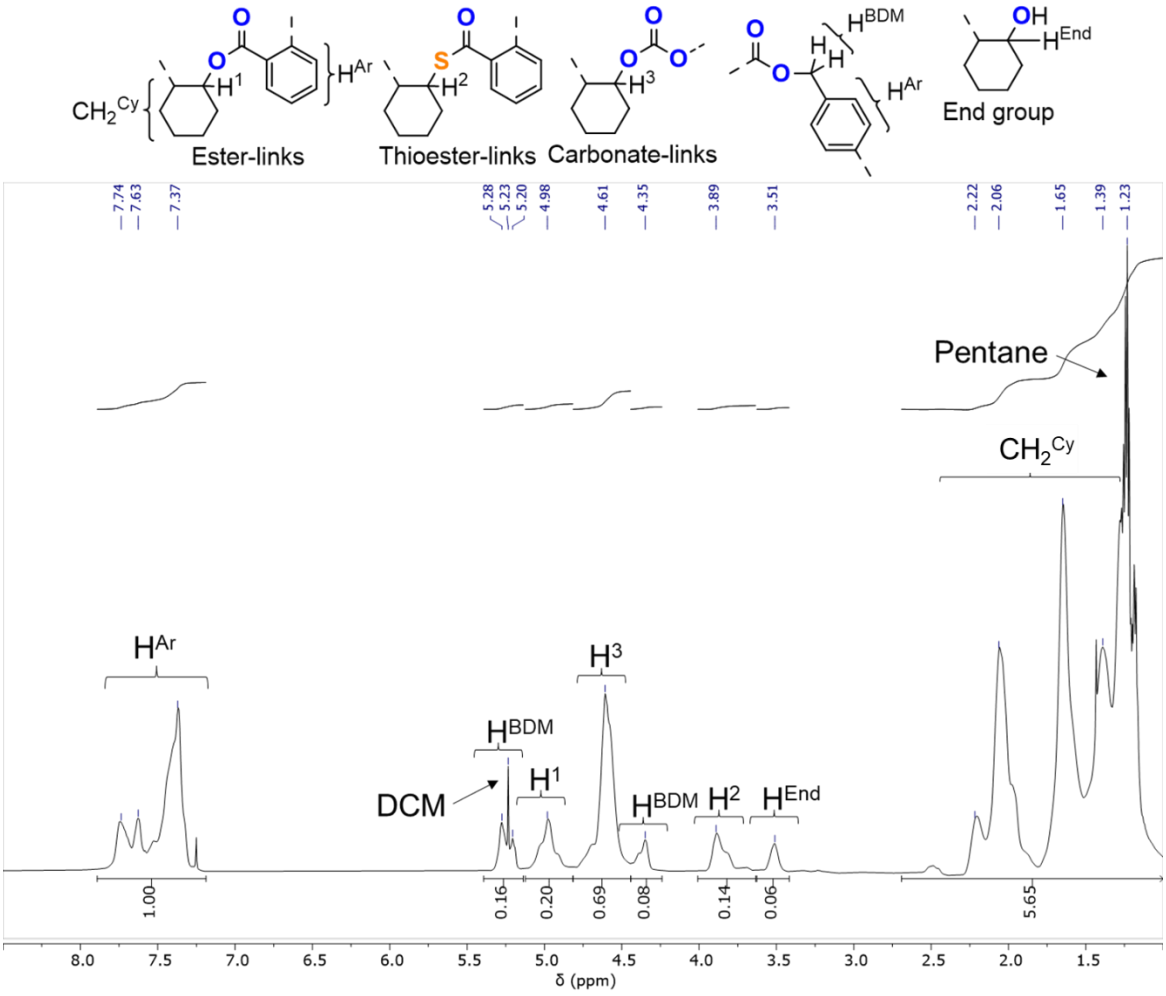

Figure S 20: ^{1}H NMR spectrum (600 MHz, 25°C, $CDCl_3$) of the terpolymer corresponding table 1, run #10 with the addition of 20 equiv. 1,4-Benzendimethanol acting as a chain transfer agent.

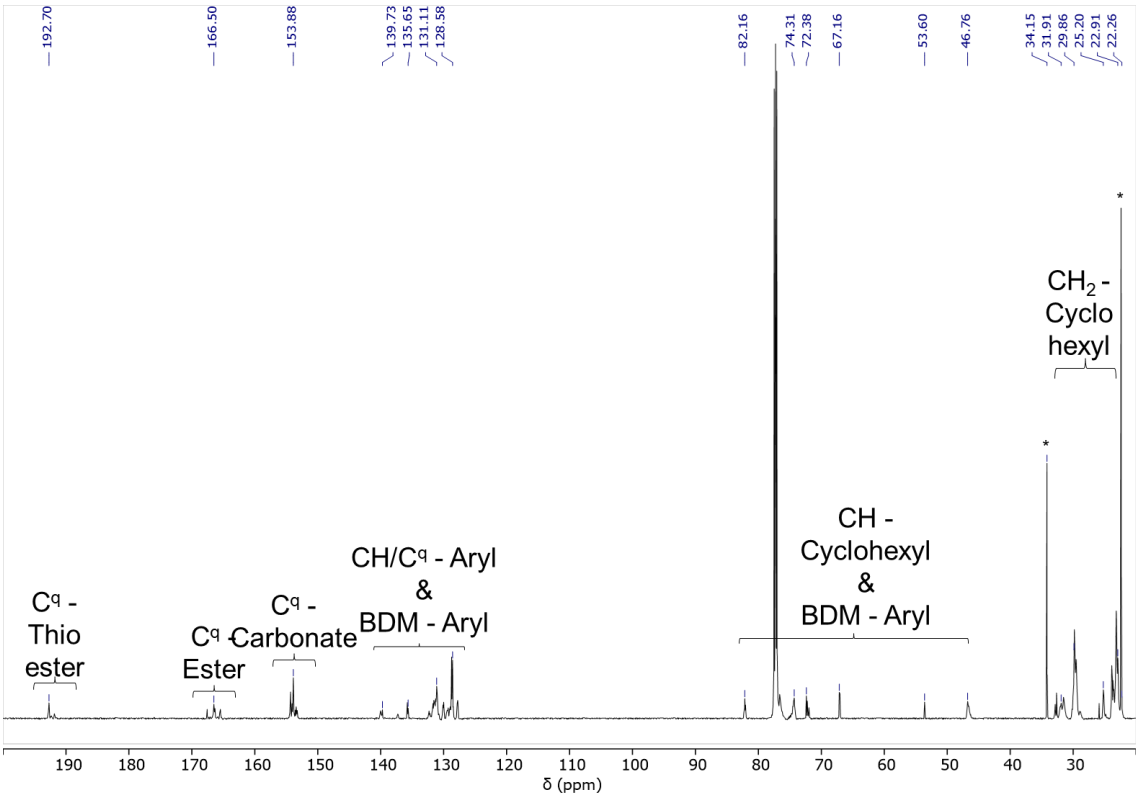

Figure S 21: ^{13}H NMR spectrum (151 MHz, 25°C, $CDCl_3$) of the terpolymer corresponding table 1, run #10 with the addition of 20 equiv. 1,4-Benzendimethanol acting as a chain transfer agent. *denotes residual pentane.

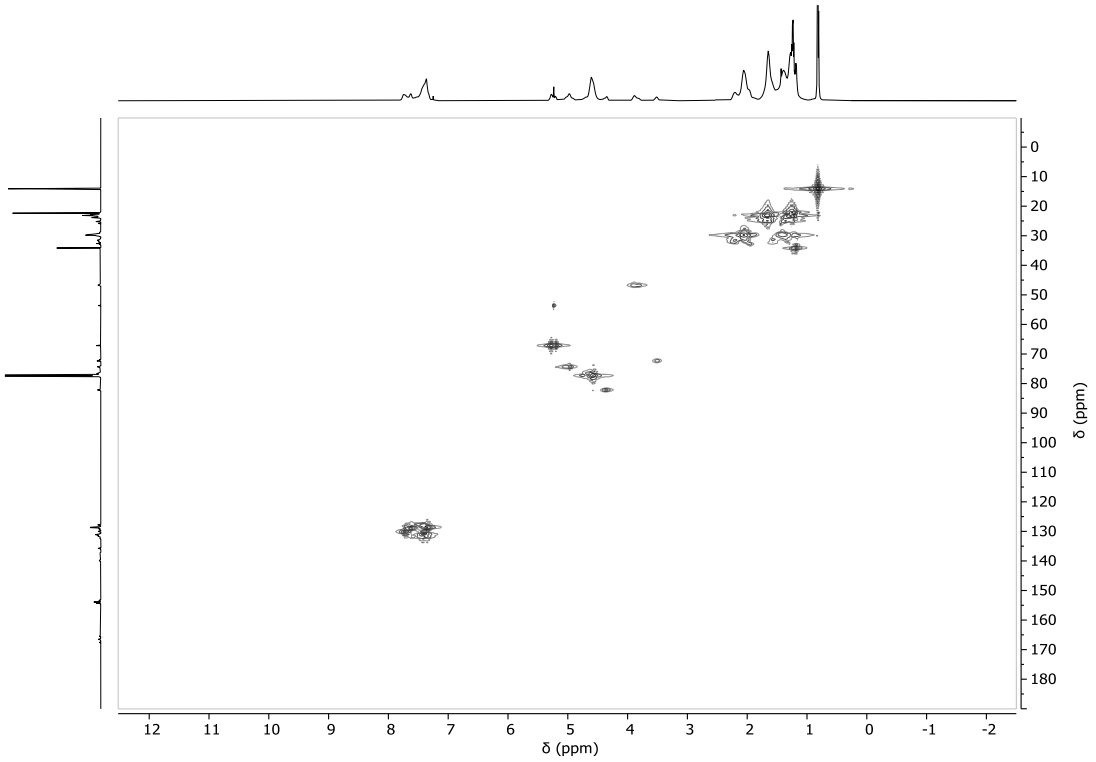

Figure S 22: ^{1}H-^{13}C HSQC NMR spectrum ($CDCl_3$, 25°C) of the terpolymer corresponding table 1, run #10 with the addition of 20 equiv. 1,4-Benzendimethanol acting as a chain transfer agent.

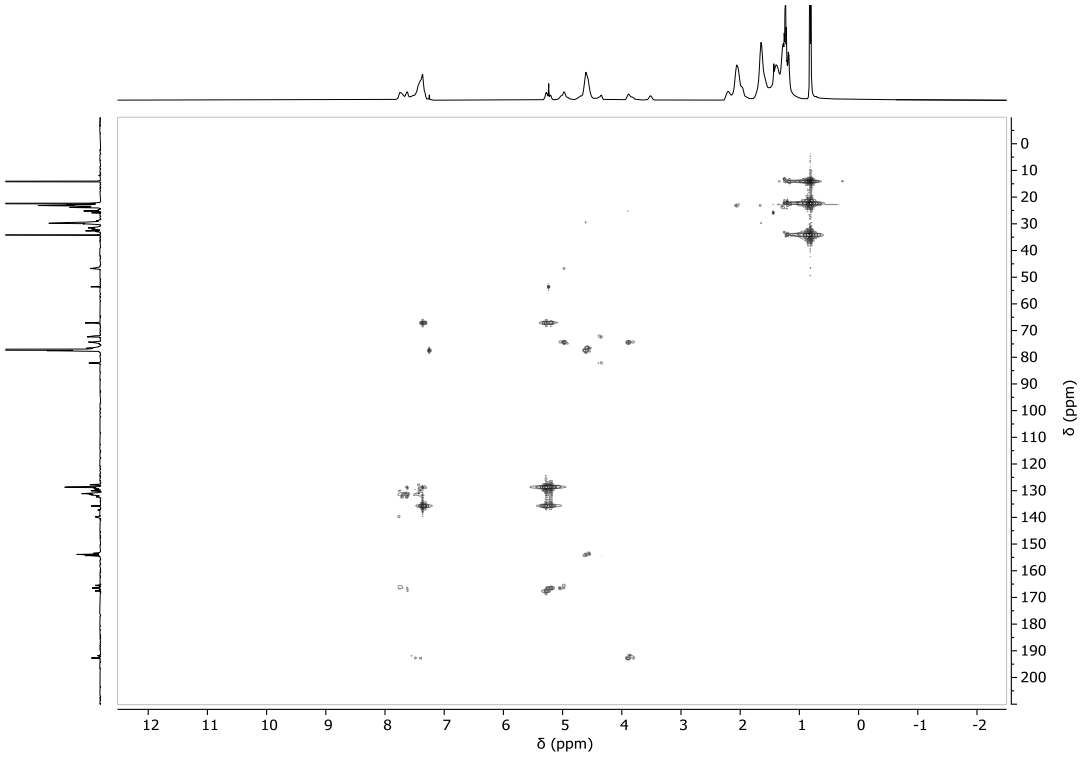

Figure S 23: ^{1}H-^{13}C HMBC NMR spectrum ($CDCl_3$, 25°C) of the terpolymer corresponding table 1, run #10 with the addition of 20 equiv. 1,4-Benzendimethanol acting as a chain transfer agent.

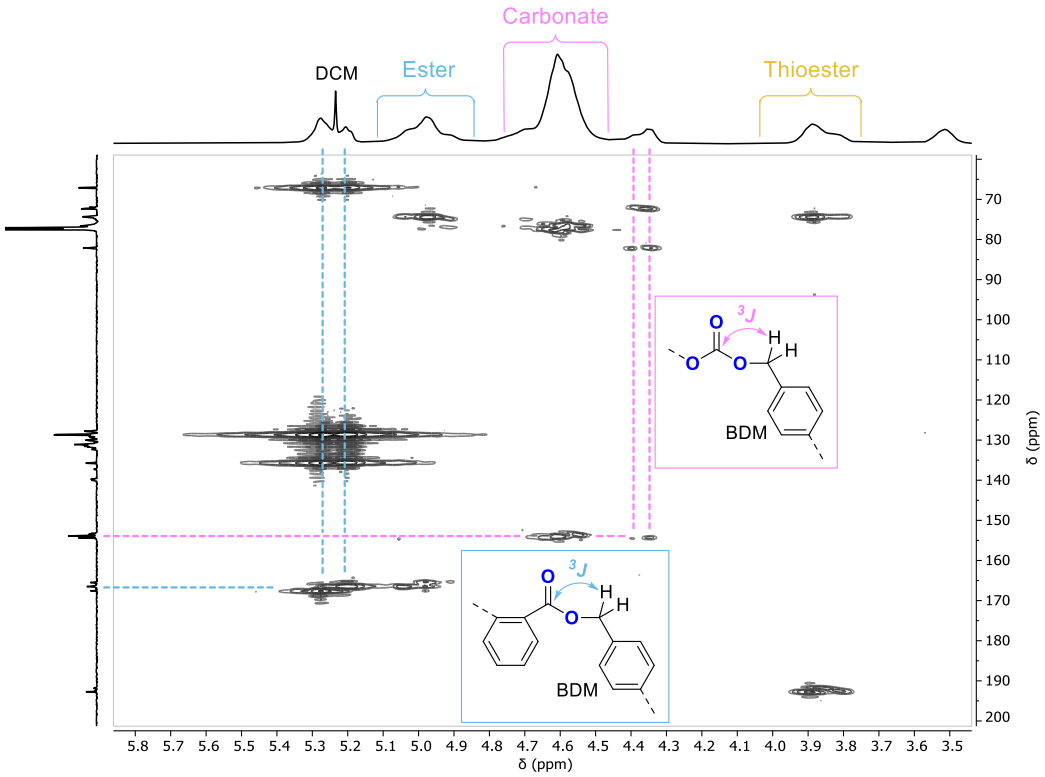

Figure S 24: Zoom into ^{1}H-^{13}C HMBC NMR spectrum (25°C, $CDCl_3$) of the terpolymer corresponding table 1, run #10 with the addition of 20 equiv. 1,4-Benzendimethanol acting as a chain transfer agent showing that BDM has been incorporated into the polymer structure**.**

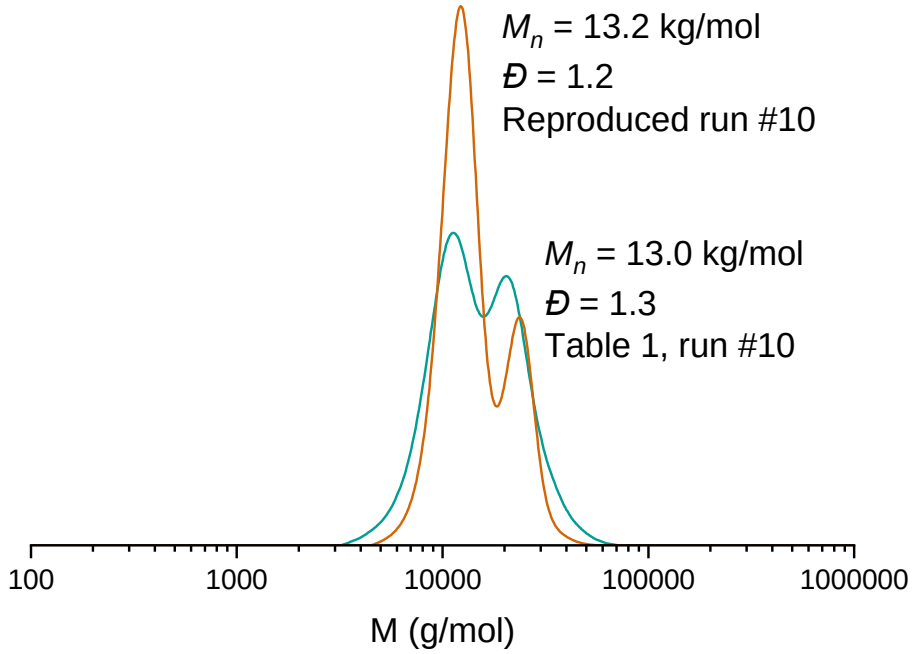

Figure S 25: GPC traces of the terpolymer corresponding to table 1, run #10 and the terpolymer obtained from the reproduced run under identical conditions but using a different batch CHO. The plot shows reproducible M_n and *Đ* but a varying degree of bimodality.

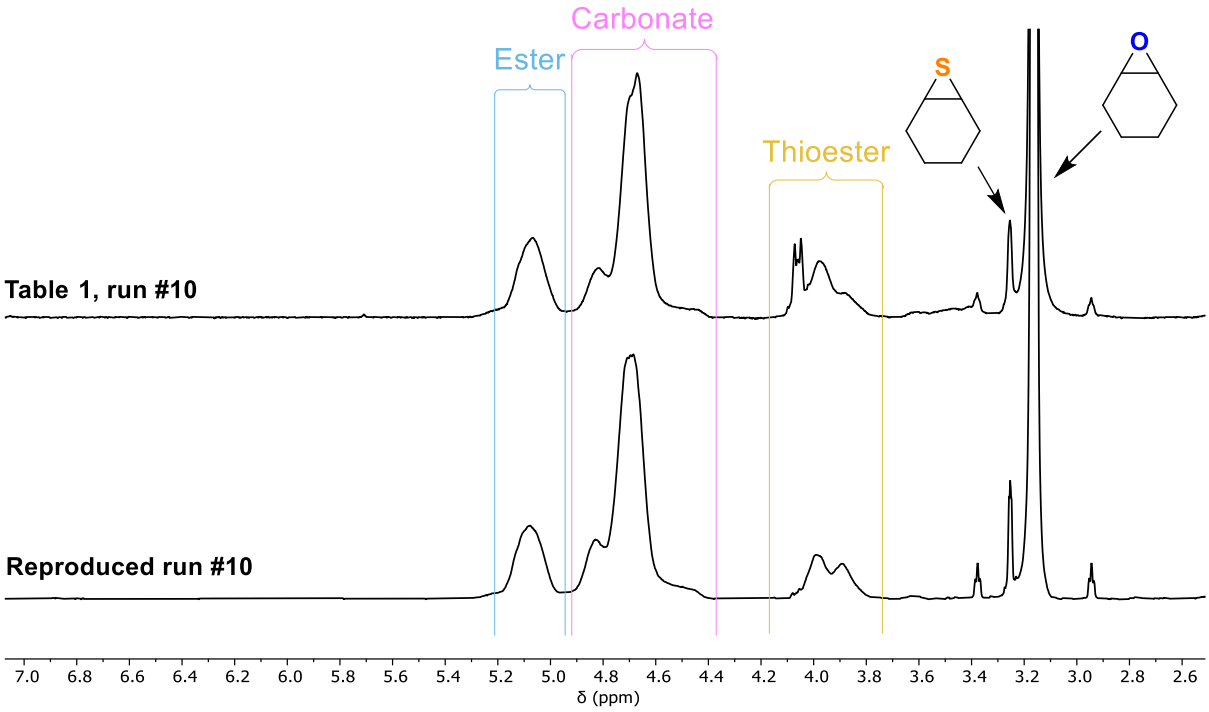

Figure S 26: Zoom into ^{1}H NMR spectrum (400 MHz, 25°C, $CDCl_3$) of the terpolymer corresponding table 1, run #10 and the terpolymer obtained from the reproduced run under identical conditions prior to workup showing the same polymer composition.

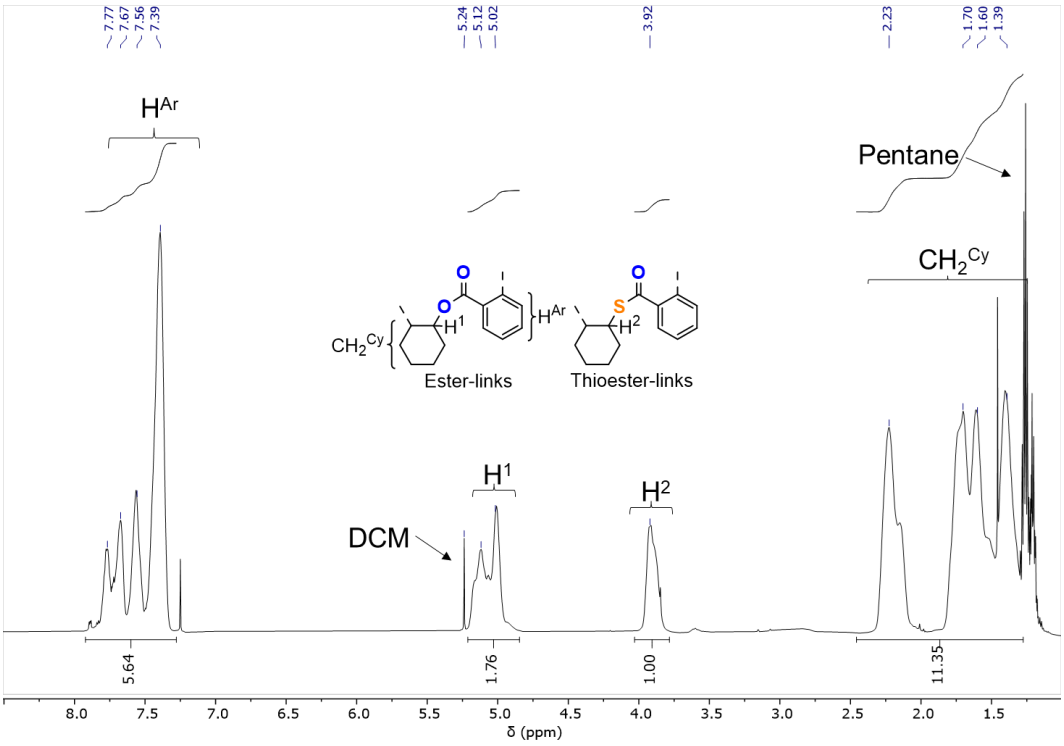

Figure S 27: ^{1}H NMR spectrum (600 MHz, 25°C, $CDCl_3$) of the copolymer obtained from PTA/CHO ROCOP showing an ester to thioester ratio of ca. 1.8 : 1.

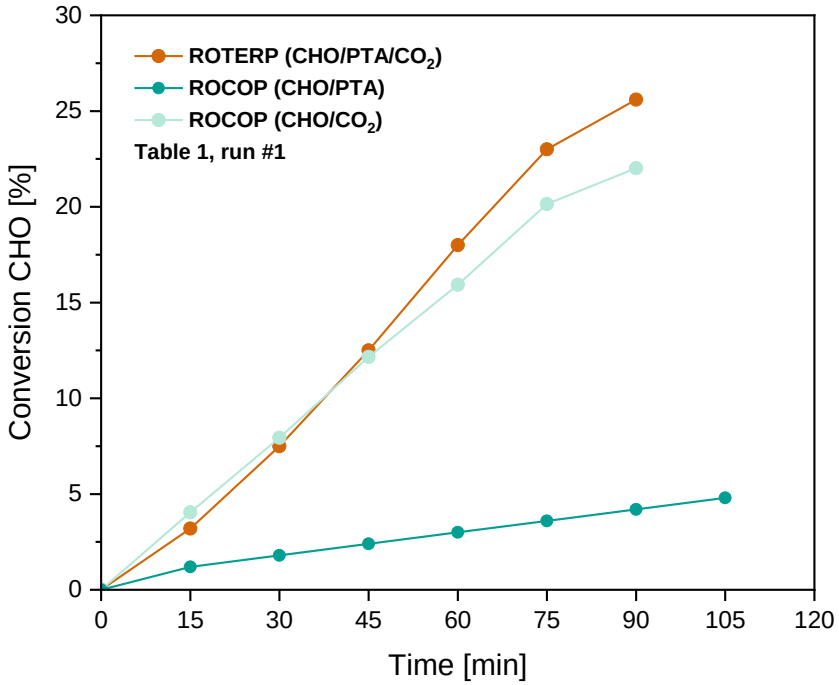

Figure S 28: Conversion of CHO *versus* time plot for the ter- and copolymerisations corresponding to table 1, run #1. Relative ratio of monomer incorporation in the terpolymer: 23 % PTA (14 % ester and 9 % thioester linkages) and 77 % CO_2. Deviation from linearity was determined after 75 min for ROTERP and CHO/CO_2 ROCOP. CHO/CO_2 ROCOP kinetic data from Ref. [7].

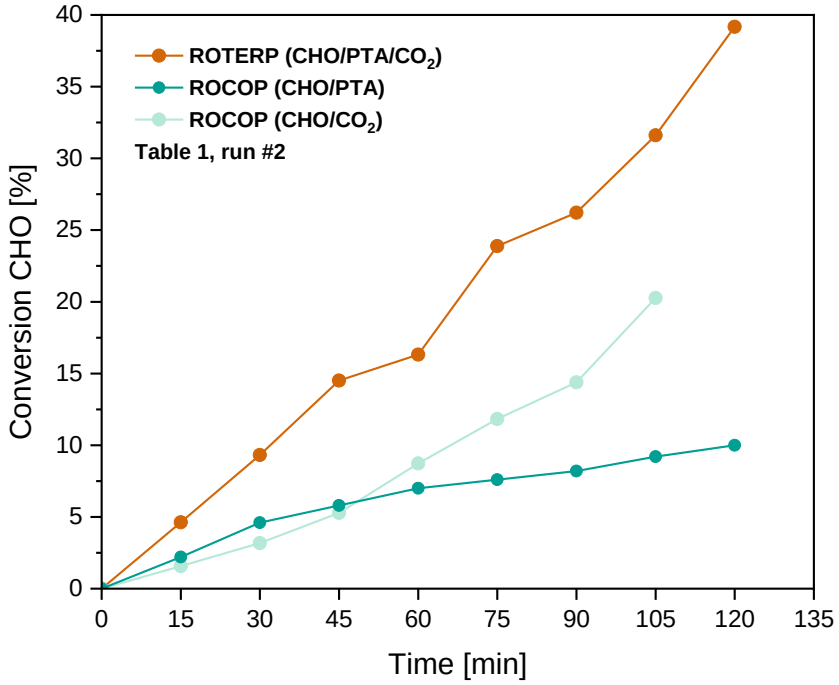

Figure S 29: Conversion of CHO *versus* time plot for the ter- and copolymerisations corresponding to table 1, run #2. Relative ratio of monomer incorporation in the terpolymer: 25 % PTA (16 % ester and 9 % thioester linkages) and 75 % CO_2. Deviation from linearity was determined after 30 min for CHO/PTA ROCOP.

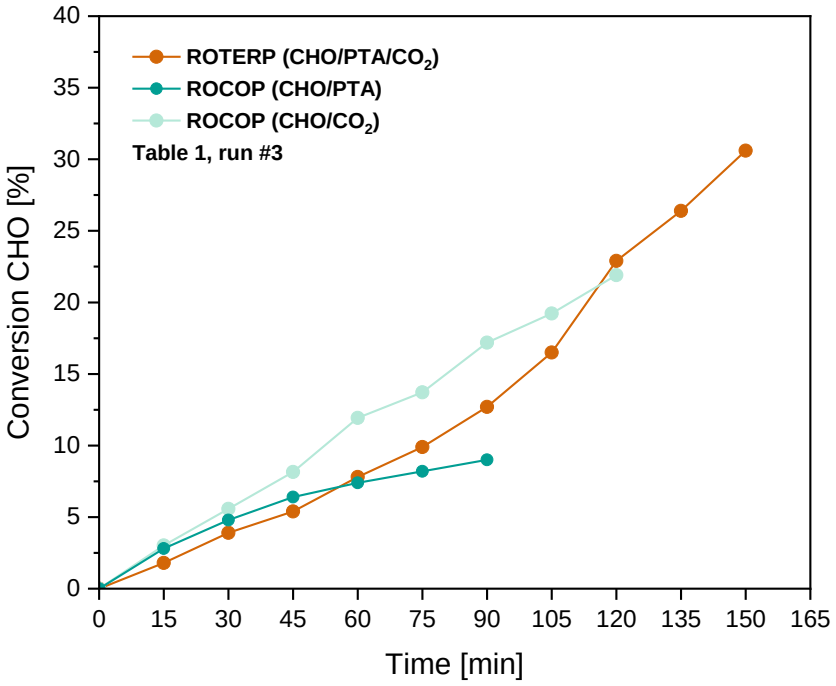

Figure S 30: Conversion of CHO *versus* time plot for the ter- and copolymerisations corresponding to table 1, run #3. Relative ratio of monomer incorporation in the terpolymer: 28 % PTA (16 % ester and 12 % thioester linkages) and 72 % CO_2. Deviation from linearity was determined after 45 min for CHO/PTA ROCOP.

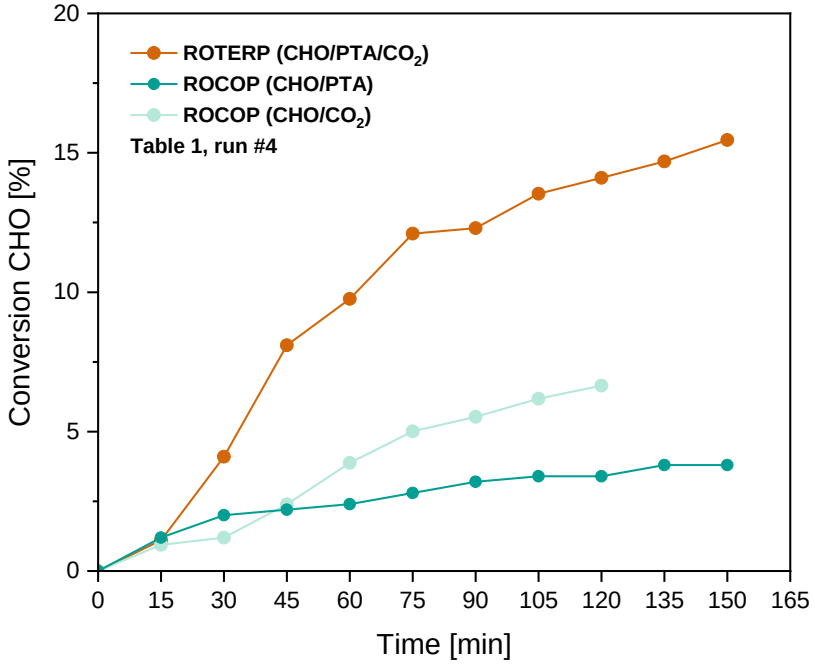

Figure S 31: Conversion of CHO *versus* time plot for the ter- and copolymerisations corresponding to table 1, run #4. Relative ratio of monomer incorporation in the terpolymer: 71 % PTA (52 % ester and 19 % thioester linkages) and 29 % CO_2. Deviation from linearity was determined after 75 min for ROTERP, 30 min for CHO/PTA ROCOP and 75 min for CHO/CO_2 ROCOP, respectively.

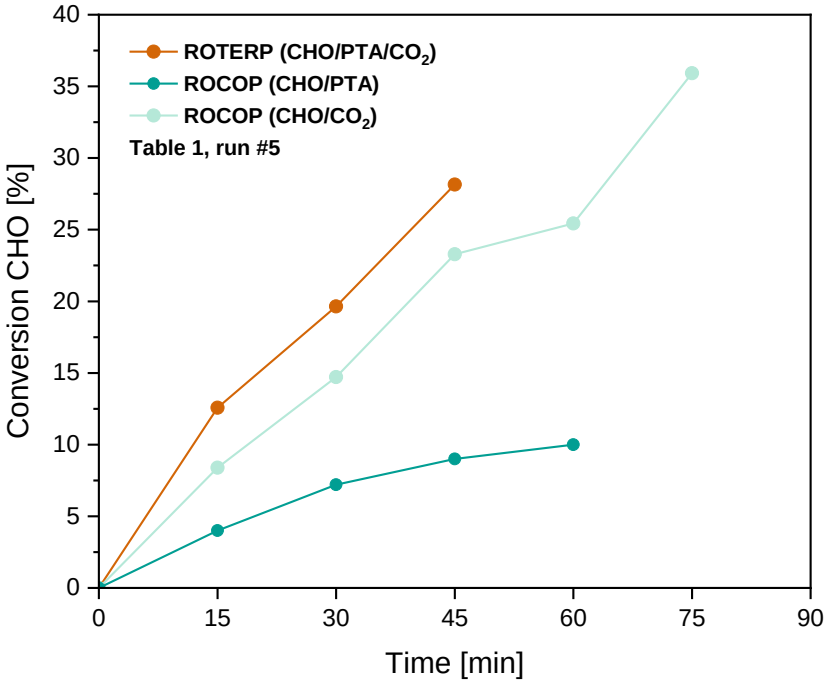

Figure S 32: Conversion of CHO *versus* time plot for the ter- and copolymerisations corresponding to table 1, run #5. Relative ratio of monomer incorporation in the terpolymer: 34 % PTA (23 % ester and 11 % thioester linkages) and 66 % CO_2. Deviation from linearity was determined after 30 min for CHO/PTA ROCOP.

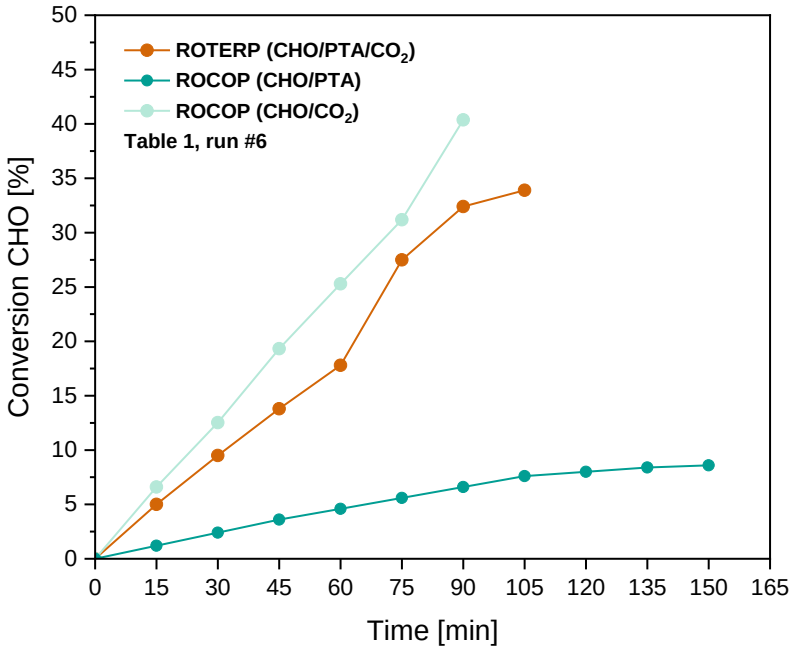

Figure S 33: Conversion of CHO *versus* time plot for the ter- and copolymerisations corresponding to table 1, run #6. Relative ratio of monomer incorporation in the terpolymer: 24 % PTA (17 % ester and 7 % thioester linkages) and 76 % CO_2. Deviation from linearity was determined after 90 min for ROTERP and 105 min for CHO/PTA ROCOP, respectively.

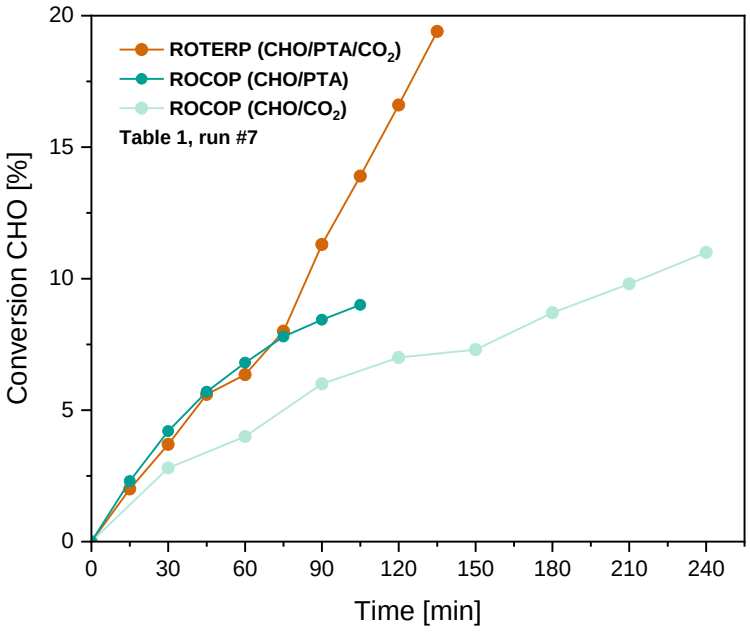

Figure S 34: Conversion of CHO *versus* time plot for the ter- and copolymerisations corresponding to table 1, run #7. Relative ratio of monomer incorporation in the terpolymer: 73 % PTA (55 % ester and 18 % thioester linkages) and 27 % CO_2. Deviation from linearity was determined after 30 min for CHO/PTA ROCOP and 90 min for CHO/CO_2 ROCOP, respectively. CHO/CO_2 ROCOP kinetic data from Ref. [7].

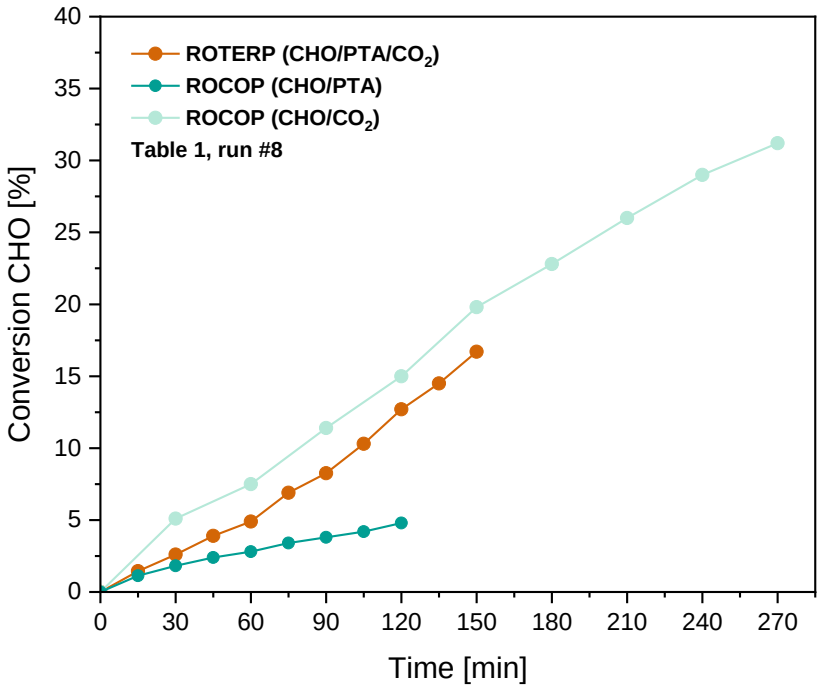

Figure S 35: Conversion of CHO *versus* time plot for the ter- and copolymerisations corresponding to table 1, run #8. Relative ratio of monomer incorporation in the terpolymer: 29 % PTA (16 % ester and 13 % thioester linkages) and 71 % CO_2. Deviation from linearity was determined after 150 min for CHO/CO_2 ROCOP. CHO/CO_2 ROCOP kinetic data from Ref. [7].

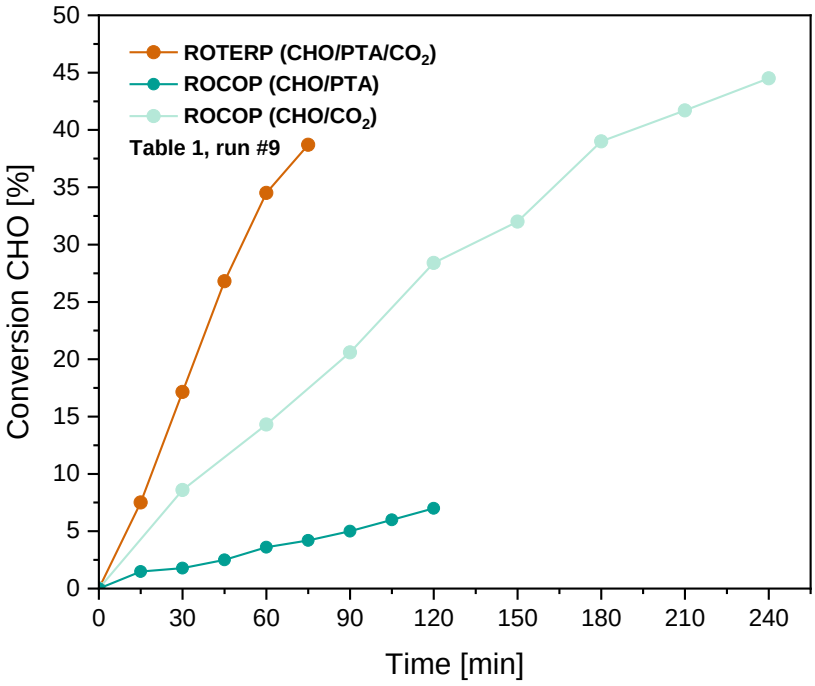

Figure S 36: Conversion of CHO *versus* time plot for the ter- and copolymerisations corresponding to table 1, run #9. Relative ratio of monomer incorporation in the terpolymer: 35 % PTA (18 % ester and 17 % thioester linkages) and 65 % CO_2. .Deviation from linearity was determined after 60 min and ROTERP and 180 min for CHO/CO_2 ROCOP, respectively. CHO/CO_2 ROCOP kinetic data from Ref. [7]

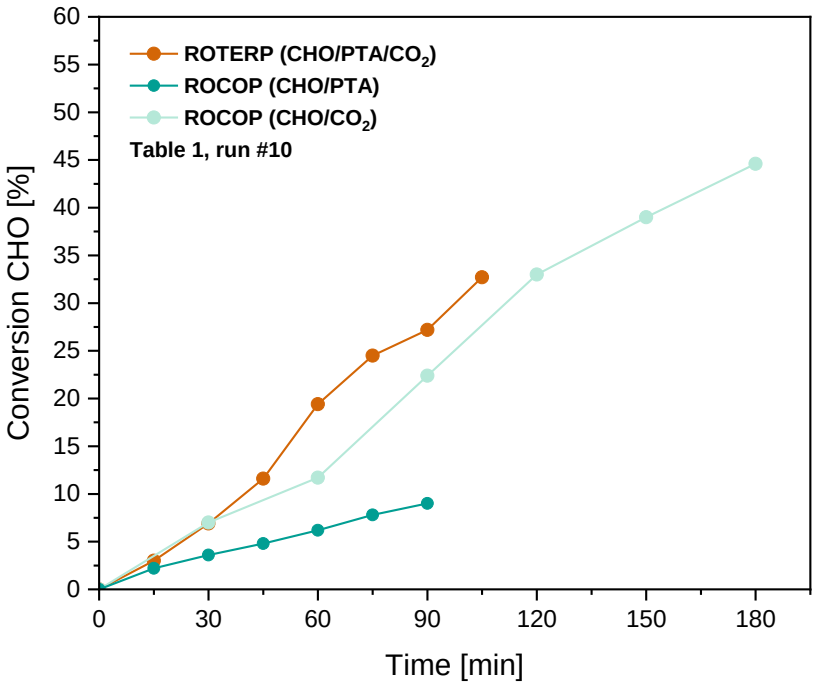

Figure S 37: Conversion of CHO *versus* time plot for the ter- and copolymerisations corresponding to table 1, run #10. Relative ratio of monomer incorporation in the terpolymer: 39 % PTA (20 % ester and 19 % thioester linkages) and 61 % CO_2. Deviation from linearity was determined after 120 min for CHO/CO_2 ROCOP. CHO/CO_2 ROCOP kinetic data from Ref. [7].

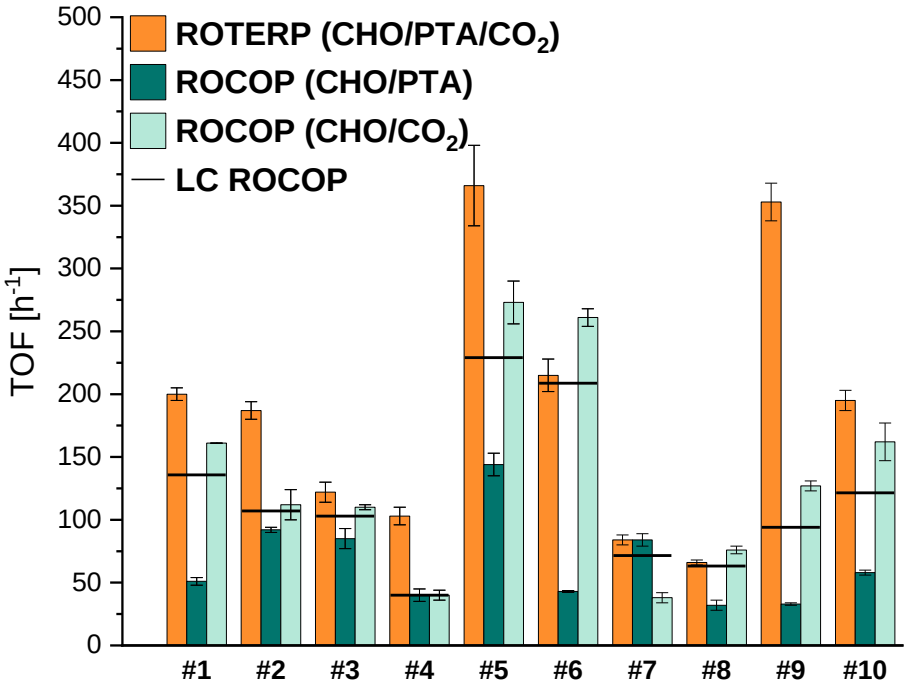

Figure S 38: Graphical comparison of the Turnover frequencies (TOFs) of the catalysts $\mathbf{L^{X}Cr^{AM}}$ (corresponding to table 1, run #1-10) in the ter- and copolymerisation and the proportionate linear combination (LC) of the TOFs in the ROCOPs.

Section S4: ROTERP results with BO

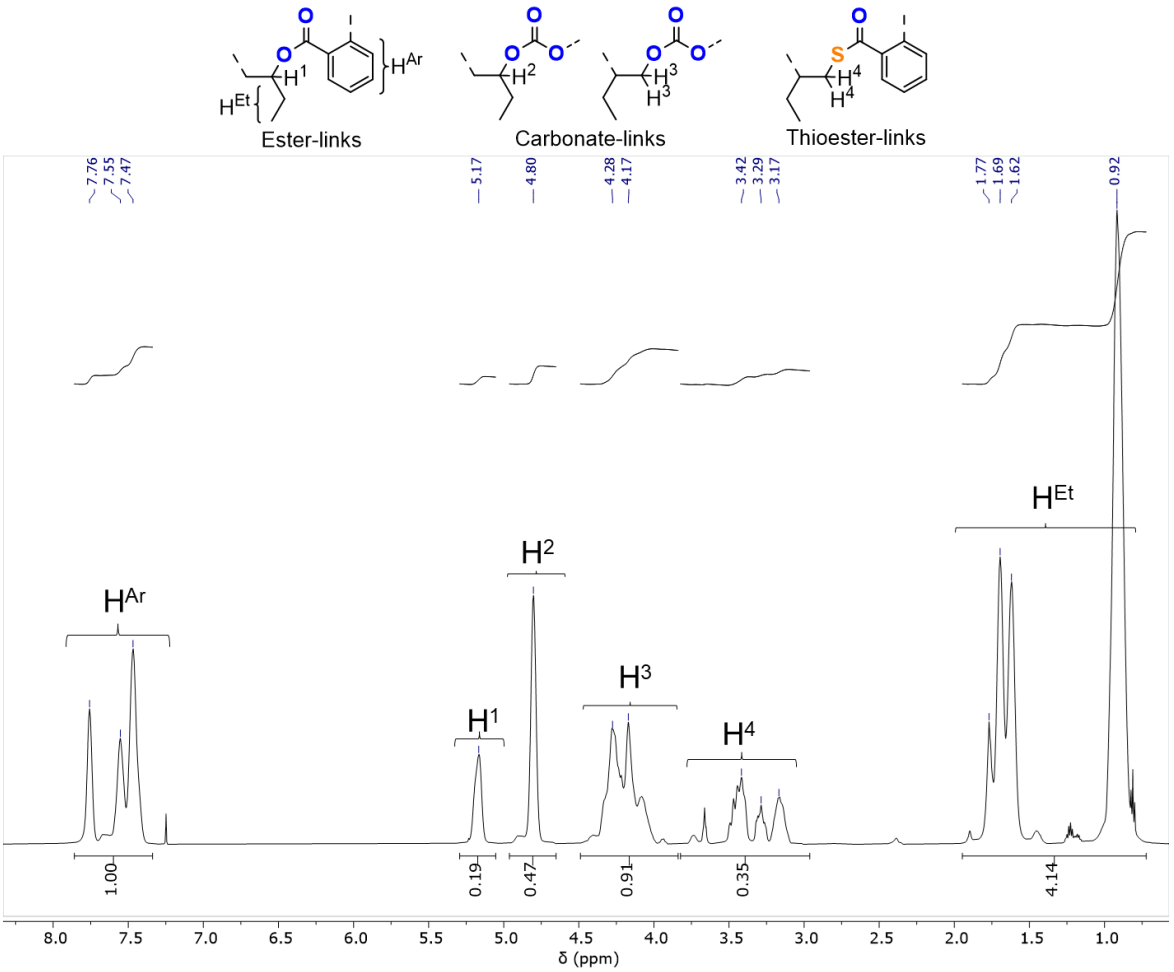

Figure S 39: ^{1}H NMR spectrum (400 MHz, $CDCl_3$, 25°C) of the precipitated polymer corresponding to table 2, run #1.

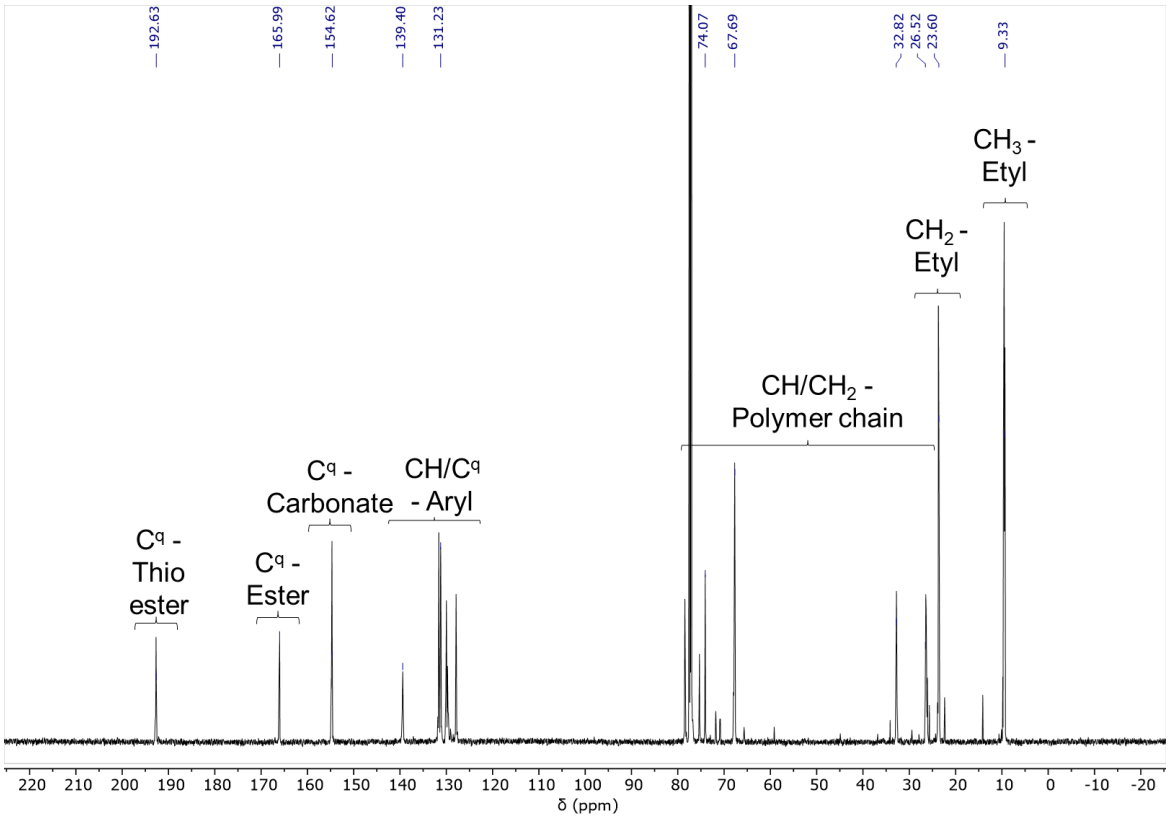

Figure S 40: ^{13}C NMR spectrum (151 MHz, $CDCl_3$, 25°C) of the precipitated polymer corresponding to table 2, run #1.

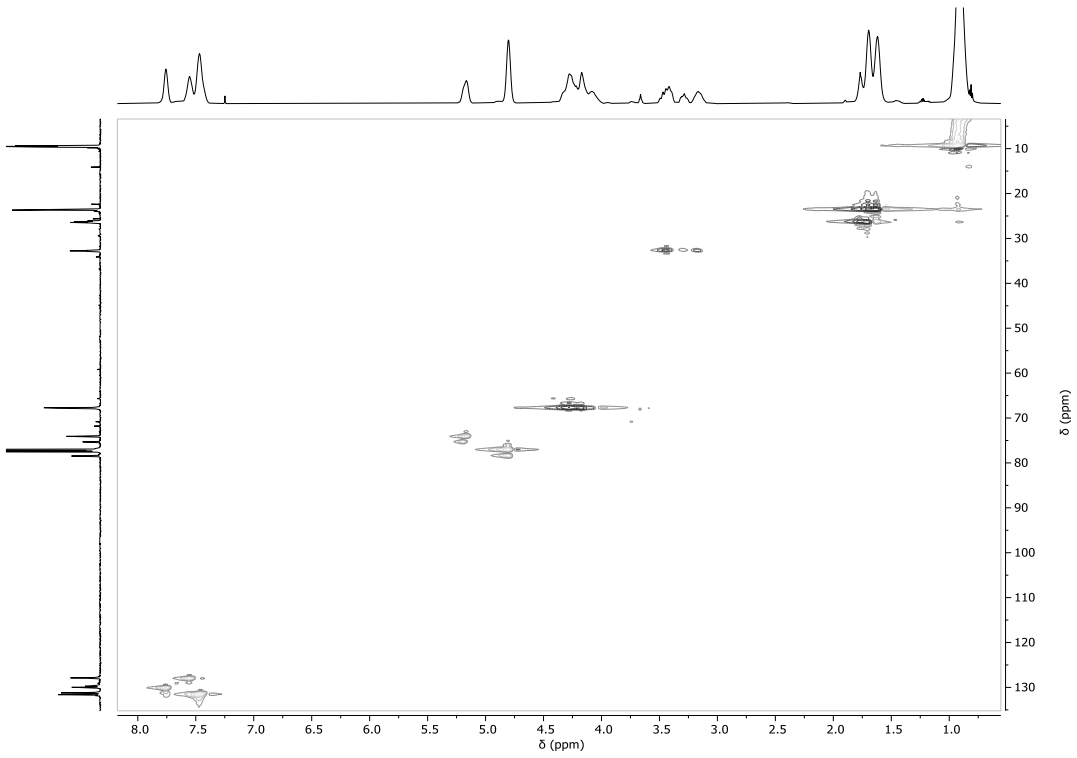

Figure S 41: ^{1}H-^{13}C HSQC NMR spectrum ($CDCl_3$, 25°C) of the precipitated polymer corresponding to table 2, run #1.

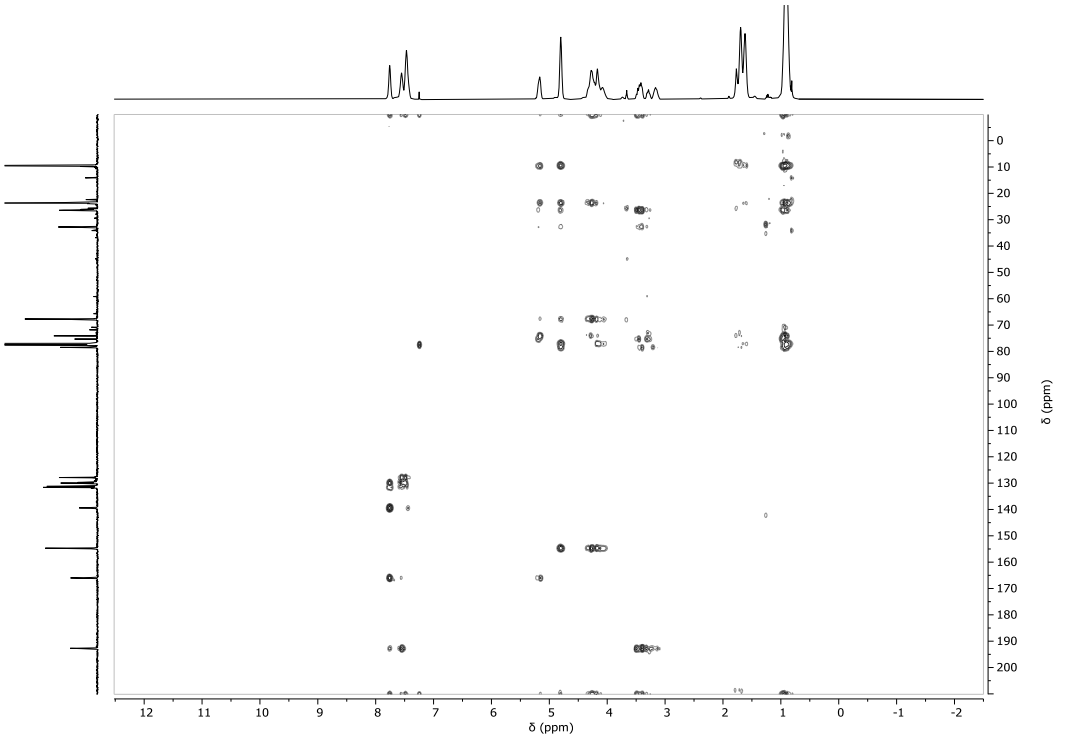

Figure S 42: ^{1}H-^{13}C HMBC NMR spectrum ($CDCl_3$, 25°C) of the precipitated polymer corresponding to table 2, run #1.

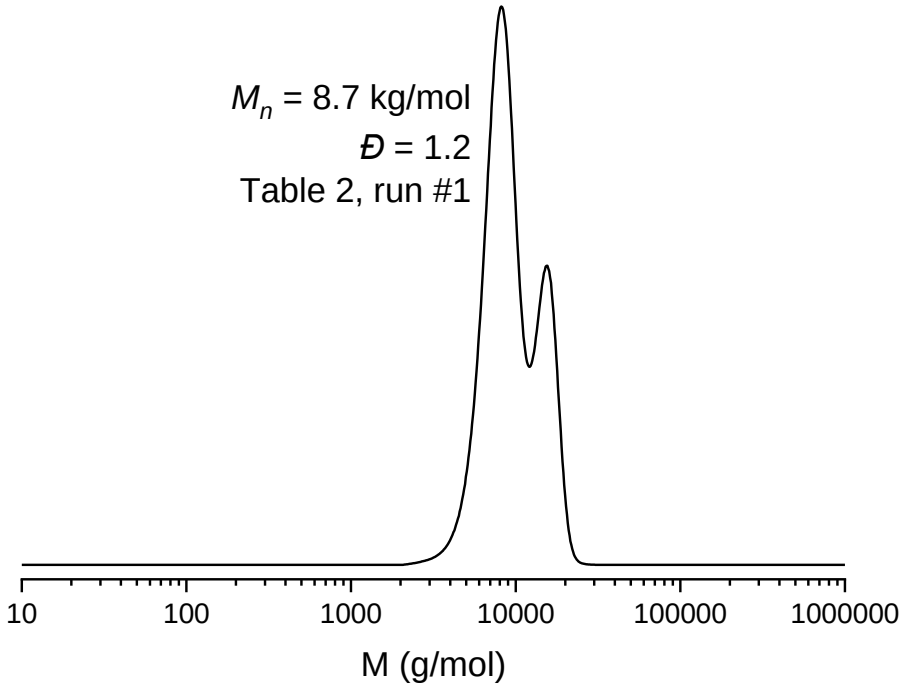

Figure S 43: GPC trace corresponding to table 2, run #1.

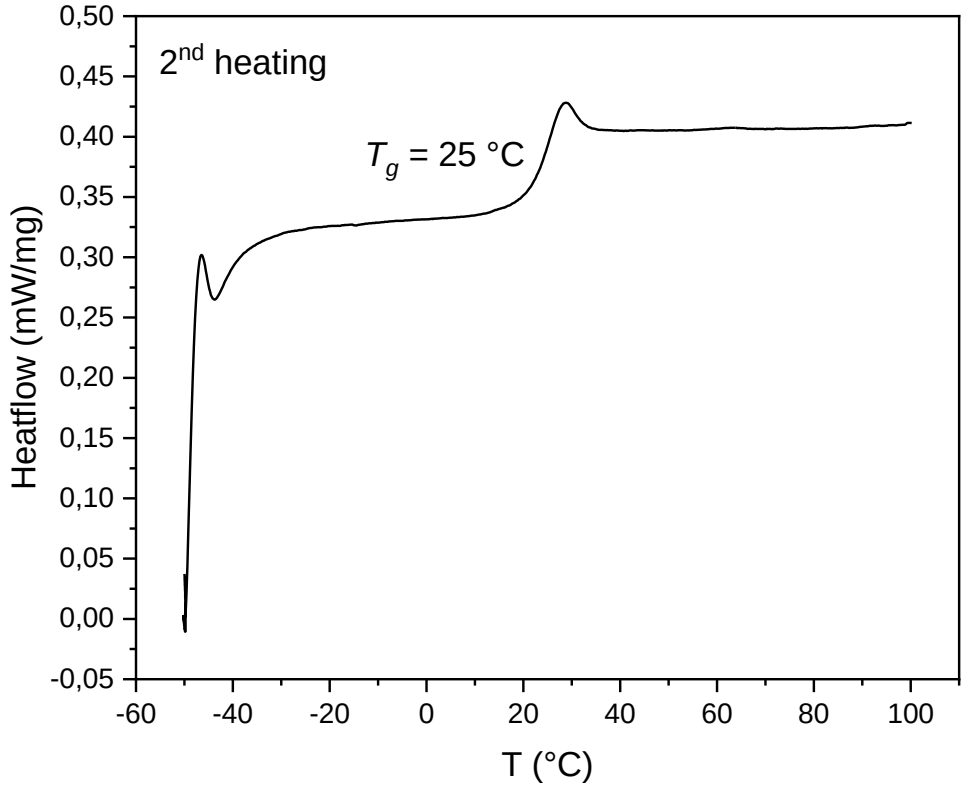

Figure S 44: DSC heating curve of the polymer corresponding table 2, run #1.

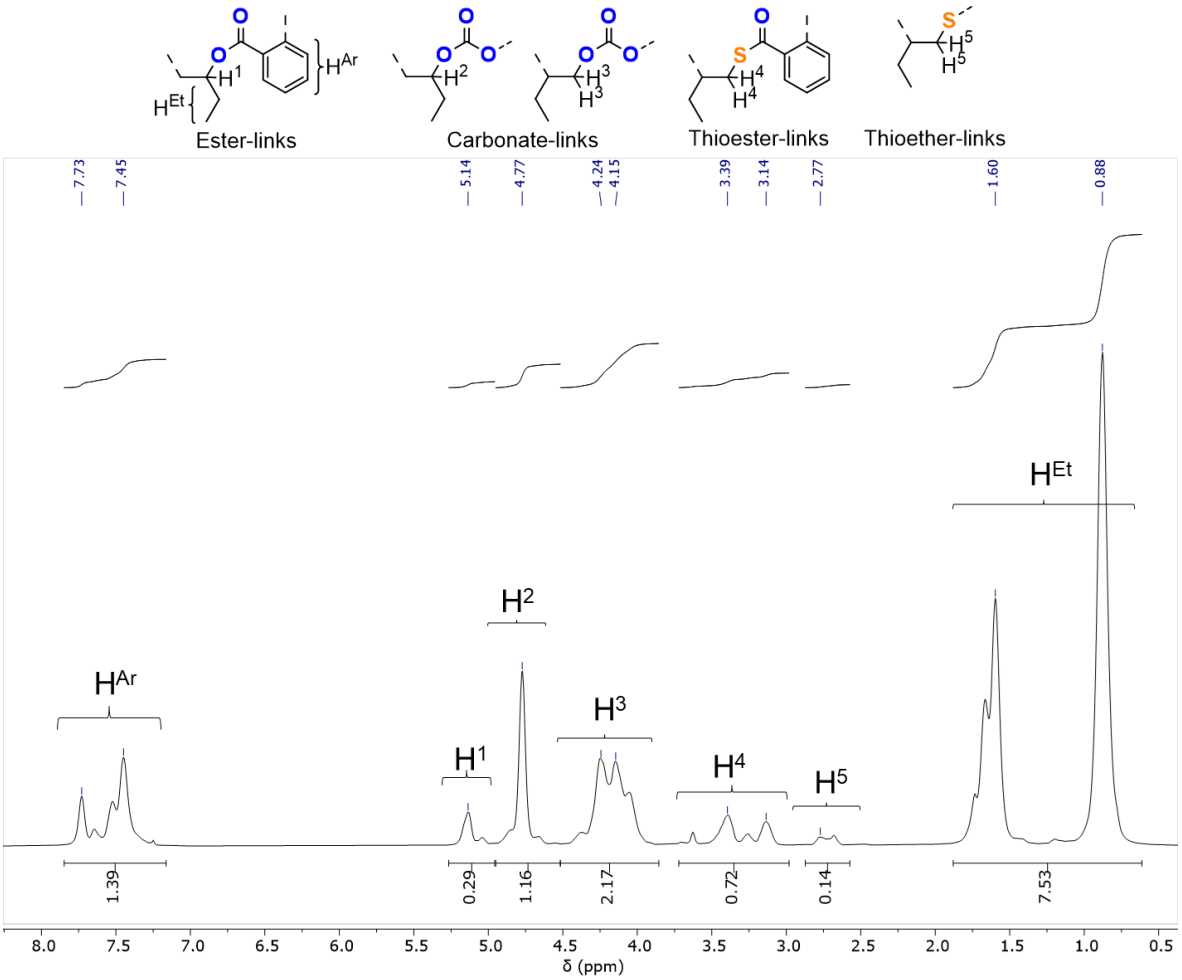

Figure S 45: ^{1}H NMR spectrum (400 MHz, $CDCl_3$, 25°C) of the precipitated polymer corresponding to table 2, run #2.

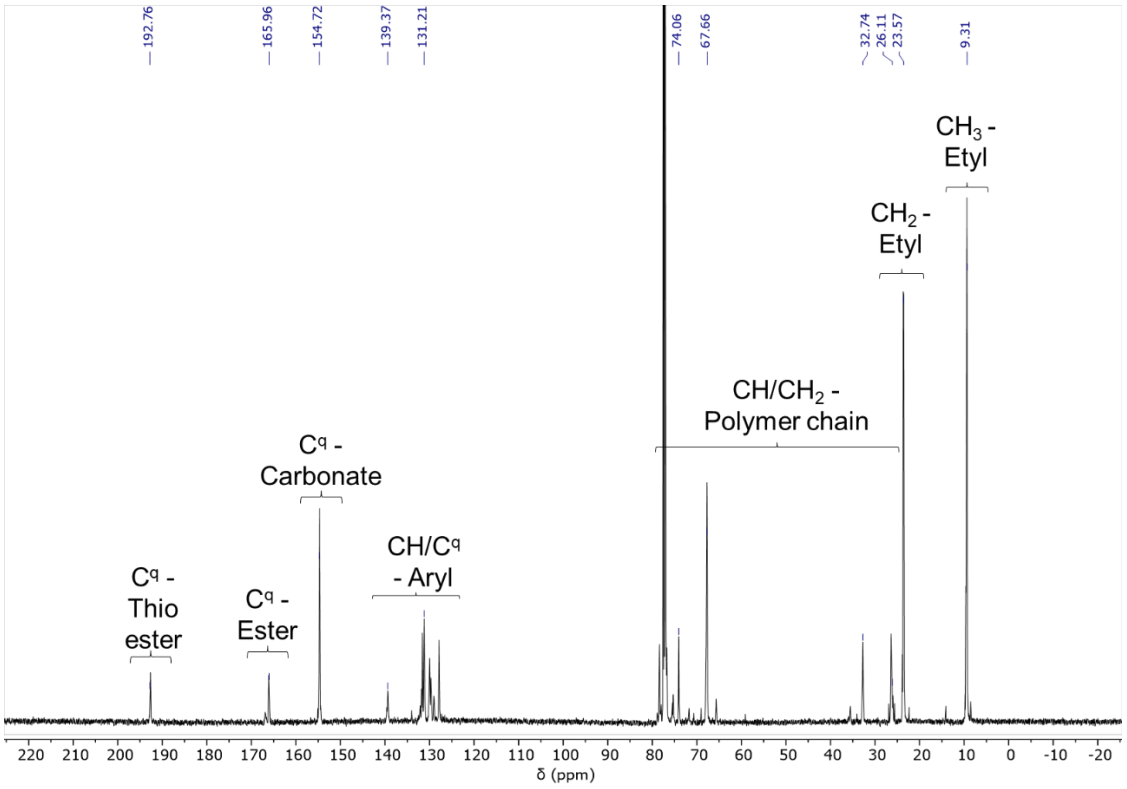

Figure S 46: ^{13}C NMR spectrum (151 MHz, $CDCl_3$, 25°C) of the precipitated polymer corresponding to table 2, run #2.

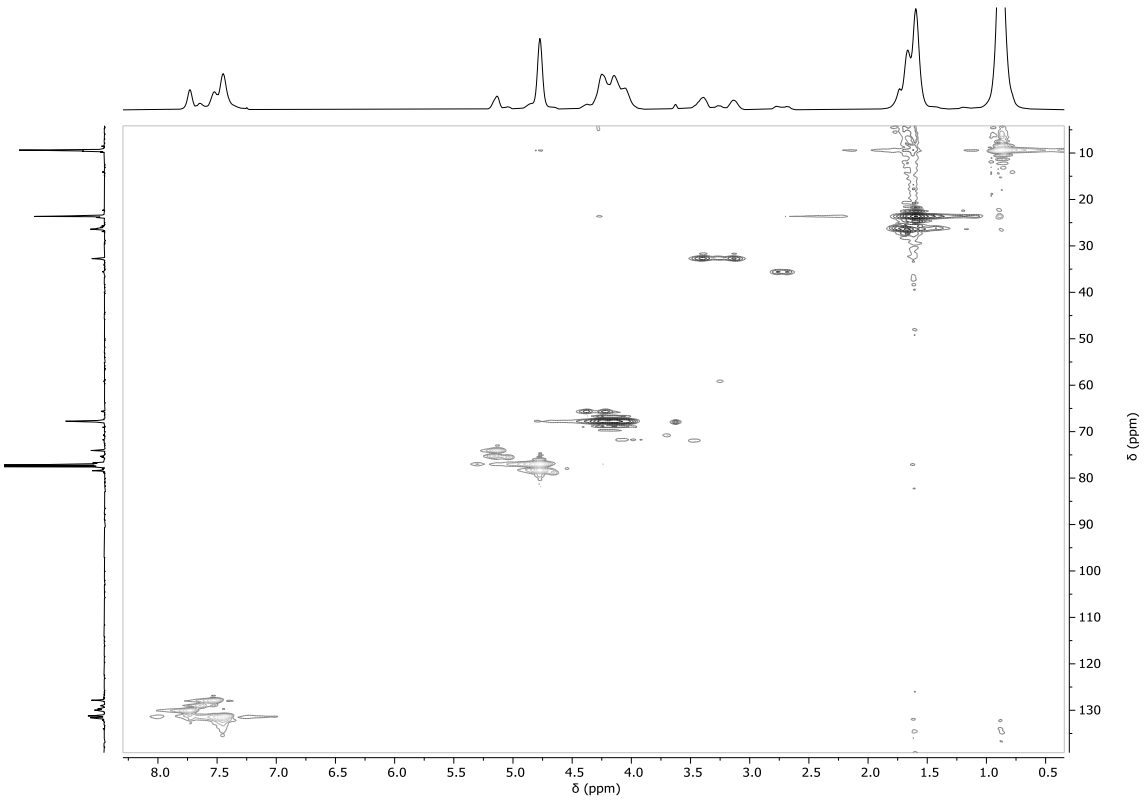

Figure S 47: ^{1}H-^{13}C HSQC NMR spectrum ($CDCl_3$, 25°C) of the precipitated polymer corresponding to table 2, run #2.

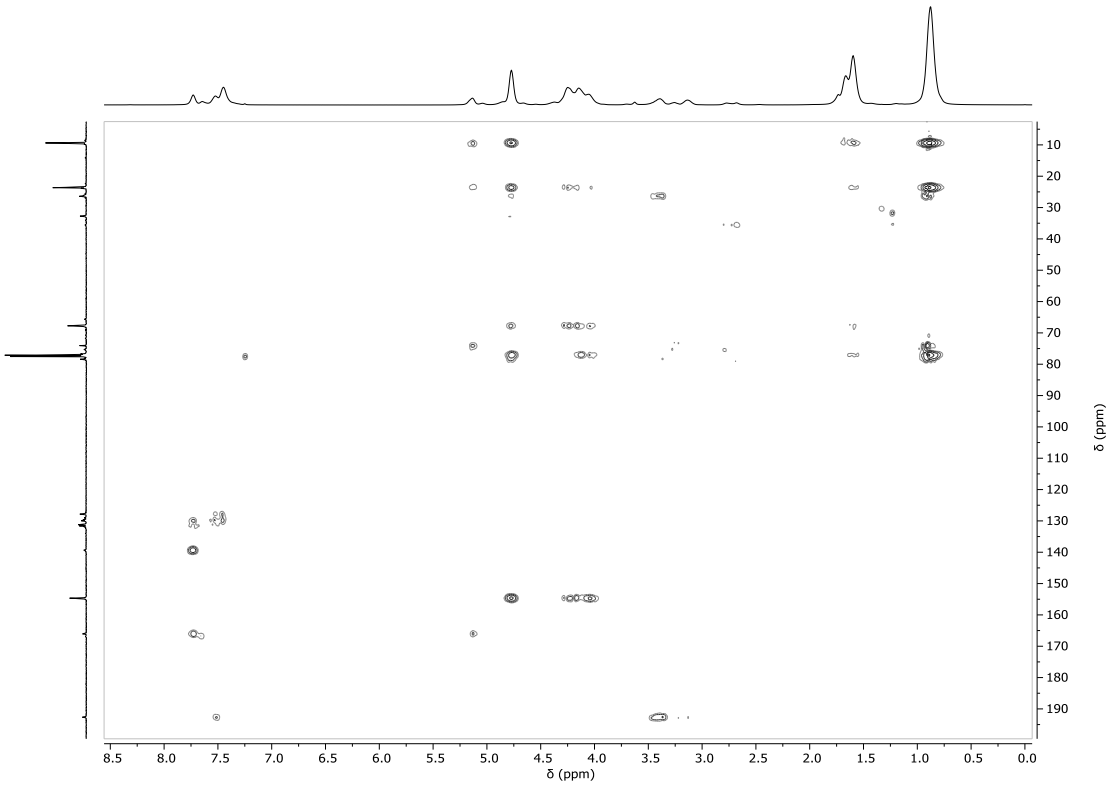

Figure S 48: ^{1}H-^{13}C HMBC NMR spectrum ($CDCl_3$, 25°C) of the precipitated polymer corresponding to table 2, run #2.

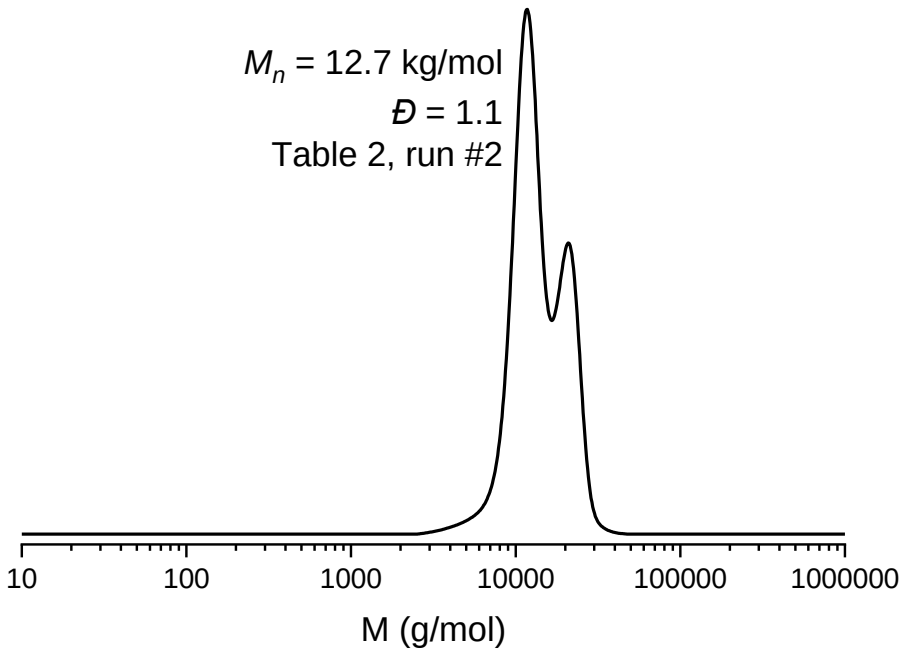

Figure S 49: GPC trace corresponding to table 2, run #2.

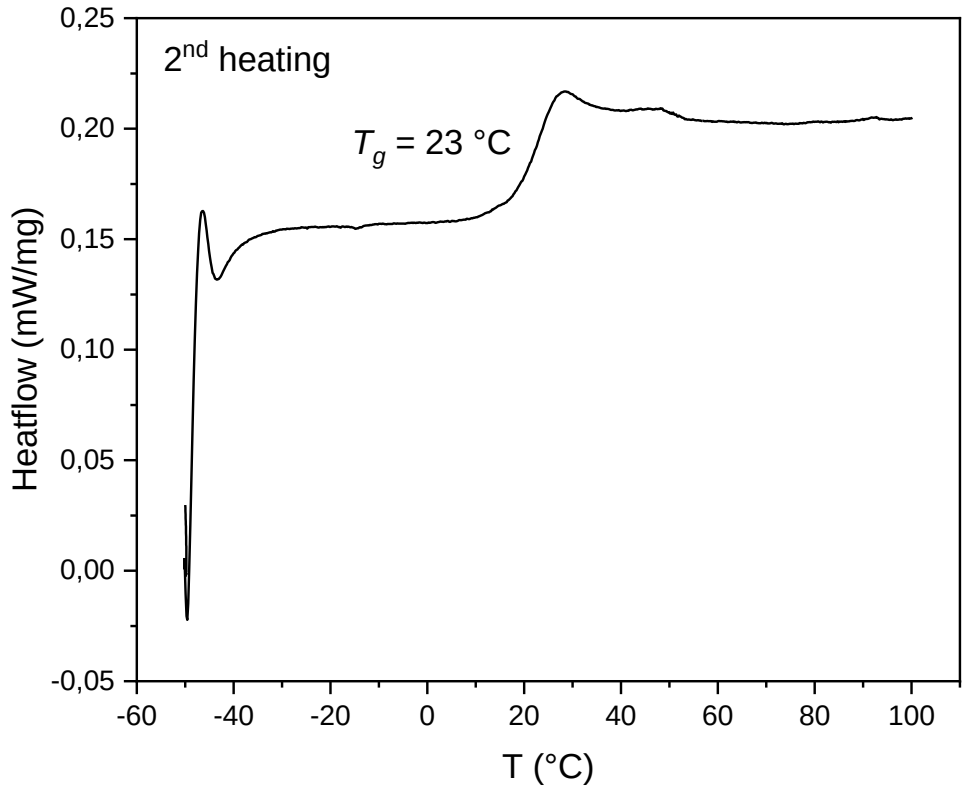

Figure S 50: DSC heating curve of the polymer corresponding table 2, run #2.

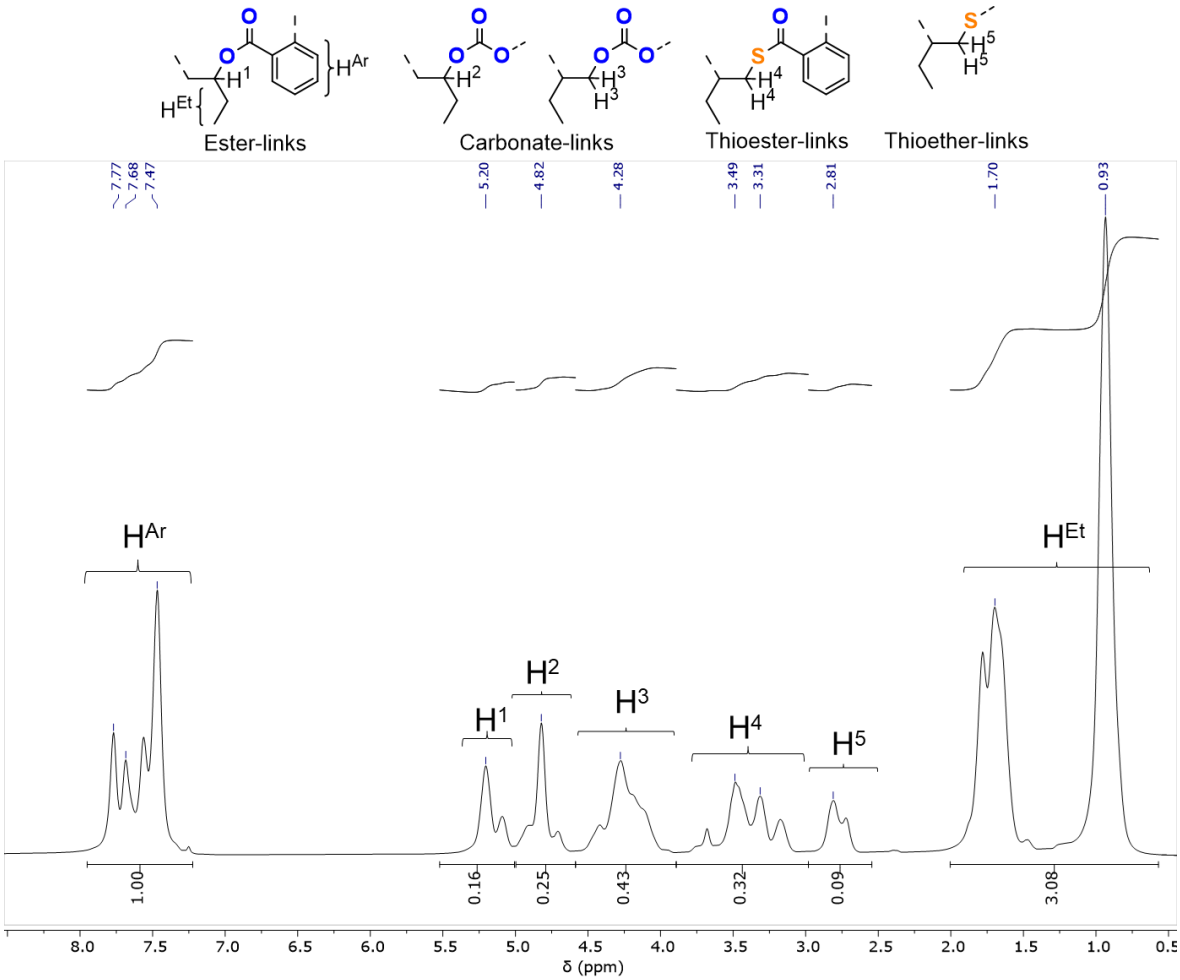

Figure S 51: ^{1}H NMR spectrum (400 MHz, $CDCl_3$, 25°C) of the precipitated polymer corresponding to table 2, run #3.

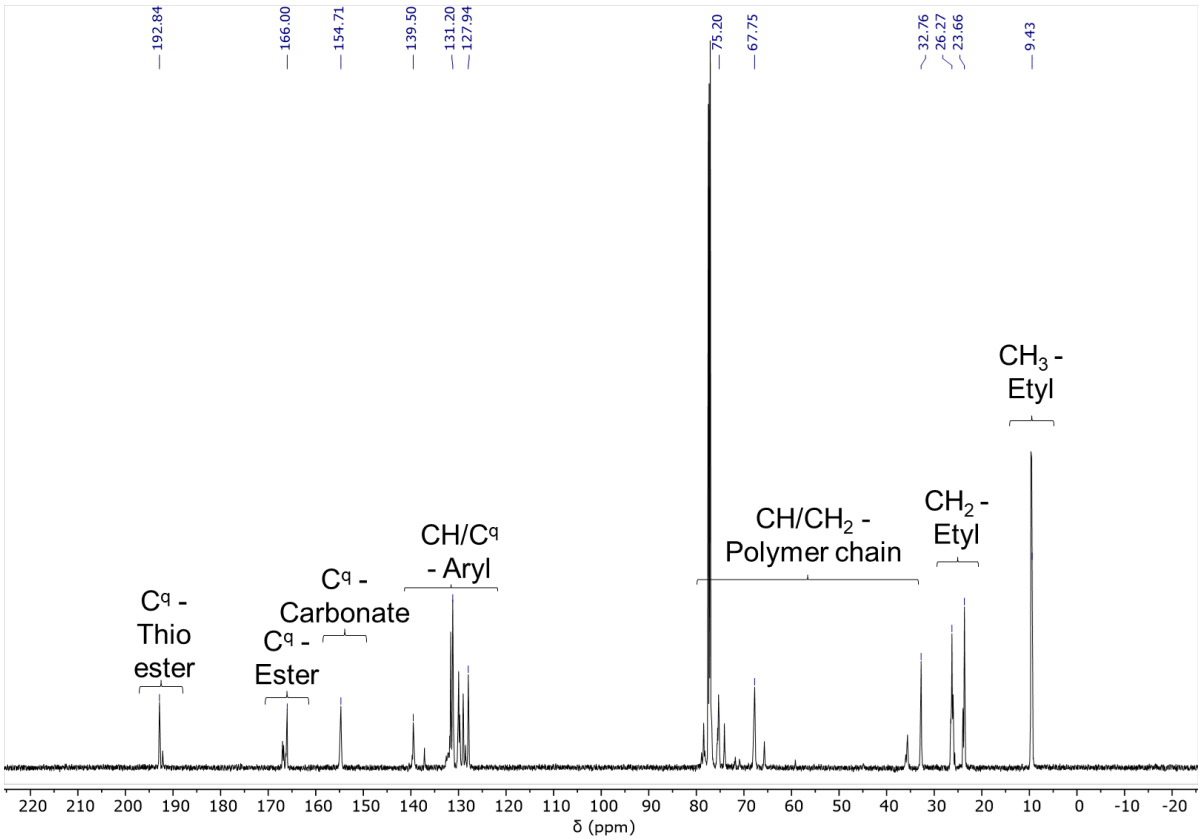

Figure S 52: ^{13}C NMR spectrum (151 MHz, $CDCl_3$, 25°C) of the precipitated polymer corresponding to table 2, run #3.

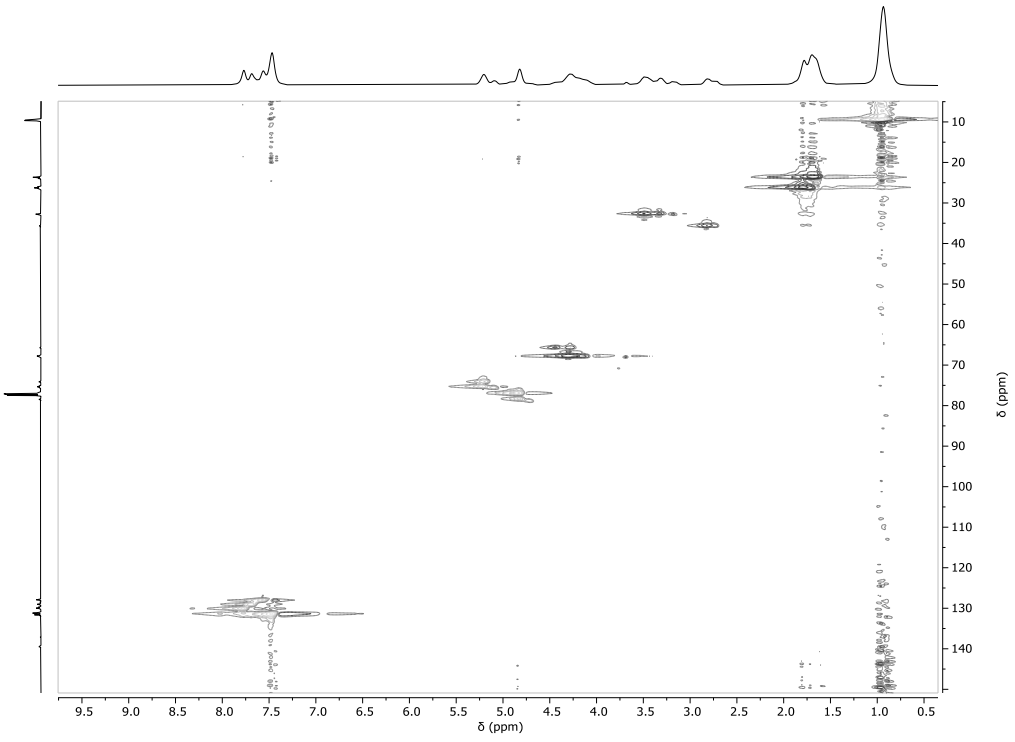

Figure S 53: ^{1}H-^{13}C HSQC NMR spectrum ($CDCl_3$, 25°C) of the precipitated polymer corresponding to table 2, run #3.

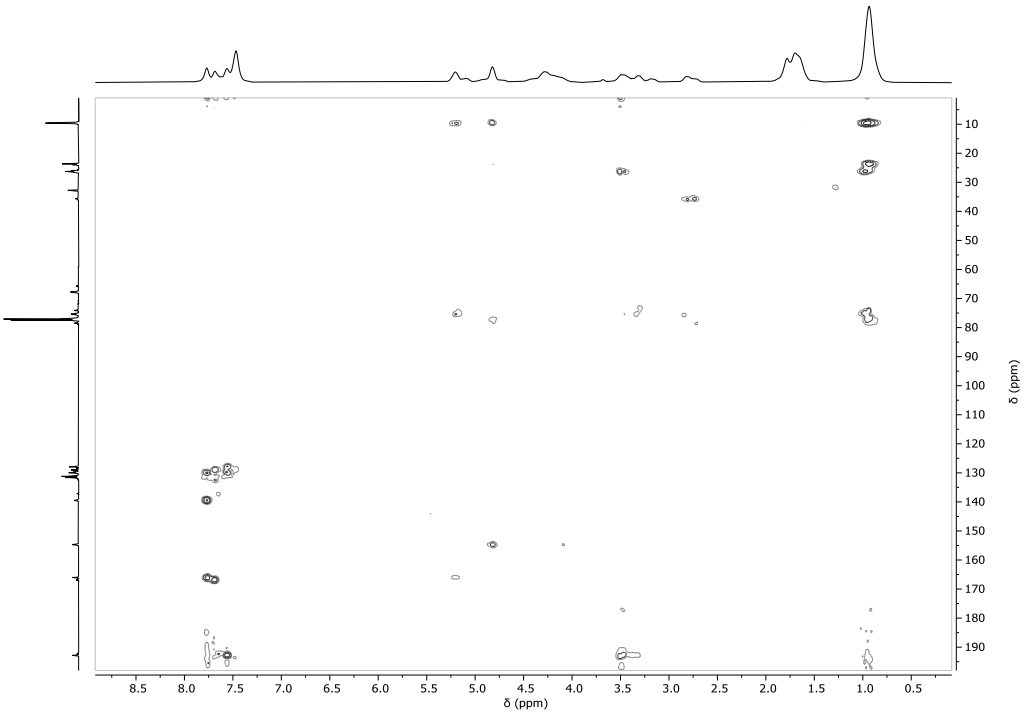

Figure S 54: ^{1}H-^{13}C HMBC NMR spectrum ($CDCl_3$, 25°C) of the precipitated polymer corresponding to table 2, run #3.

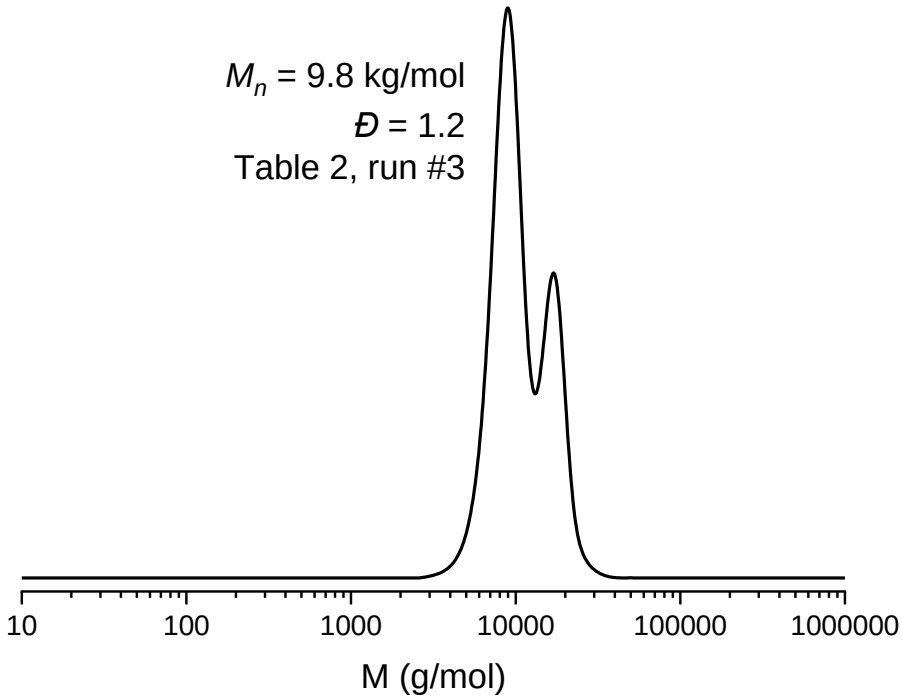

Figure S 55: GPC trace corresponding to table 2, run #3.

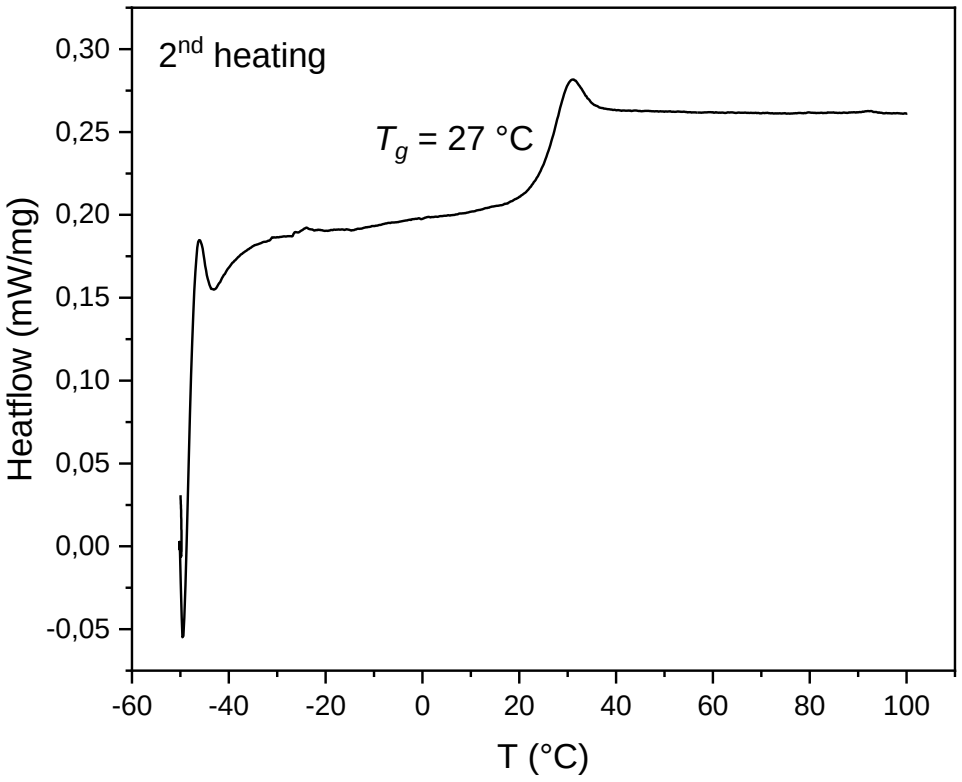

Figure S 56: DSC heating curve of the polymer corresponding table 2, run #3.

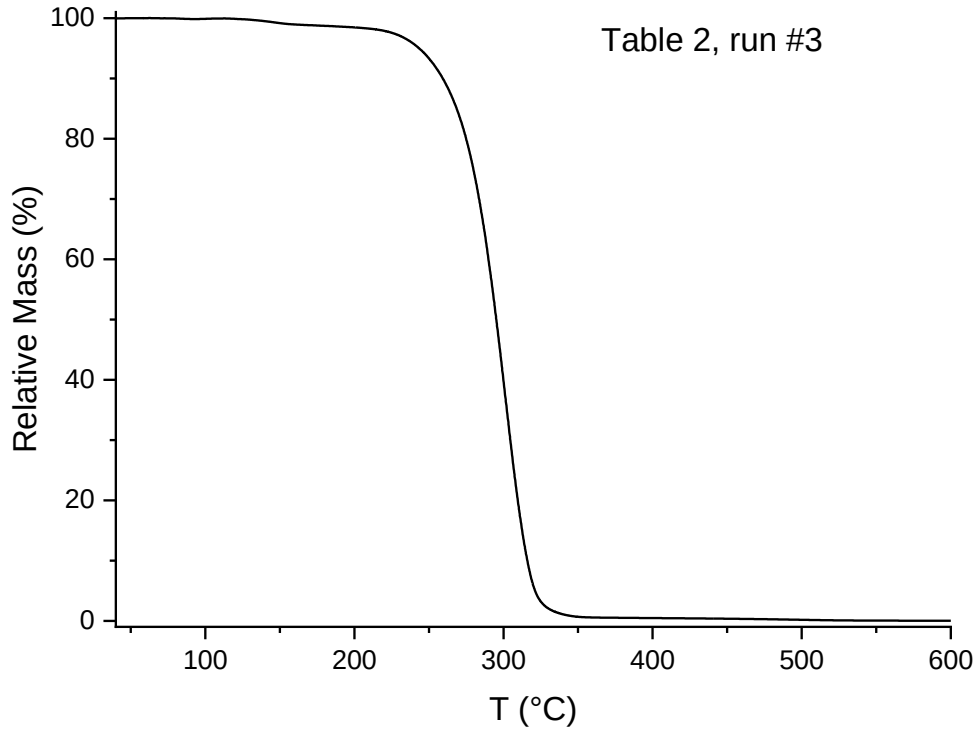

Figure S 57: TGA data of the polymer corresponding to table 2, run #3.

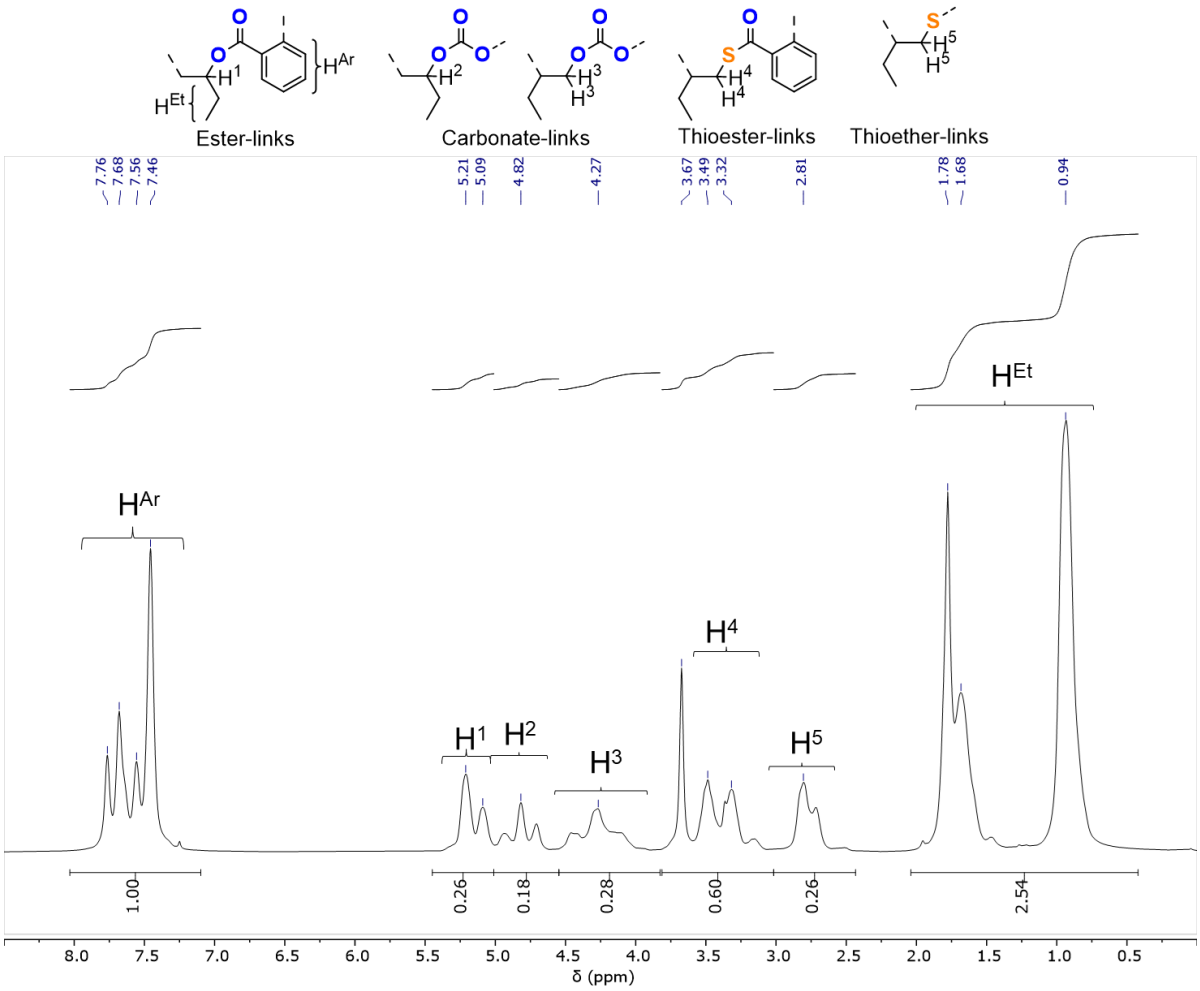

Figure S 58: ^{1}H NMR spectrum (400 MHz, $CDCl_3$, 25°C) of the precipitated polymer corresponding to table 2, run #4.

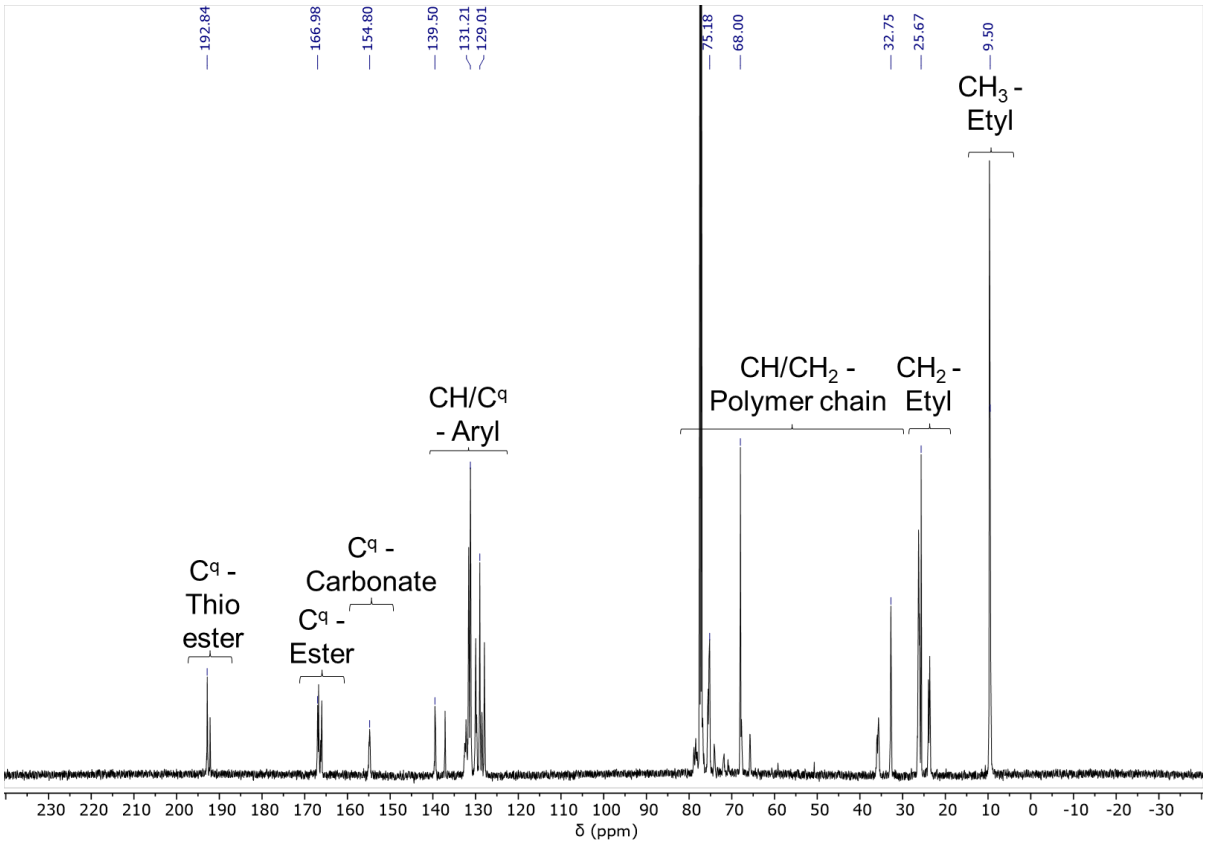

Figure S 59: ^{13}C NMR spectrum (151 MHz, $CDCl_3$, 25°C) of the precipitated polymer corresponding to table 2, run #4.

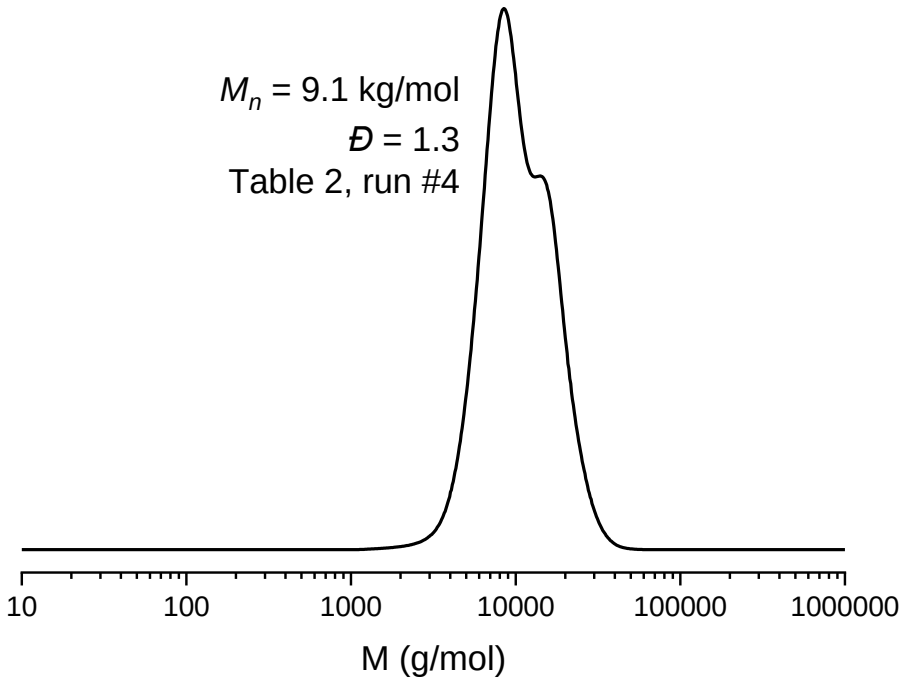

Figure S 60: GPC trace corresponding to table 2, run #4.

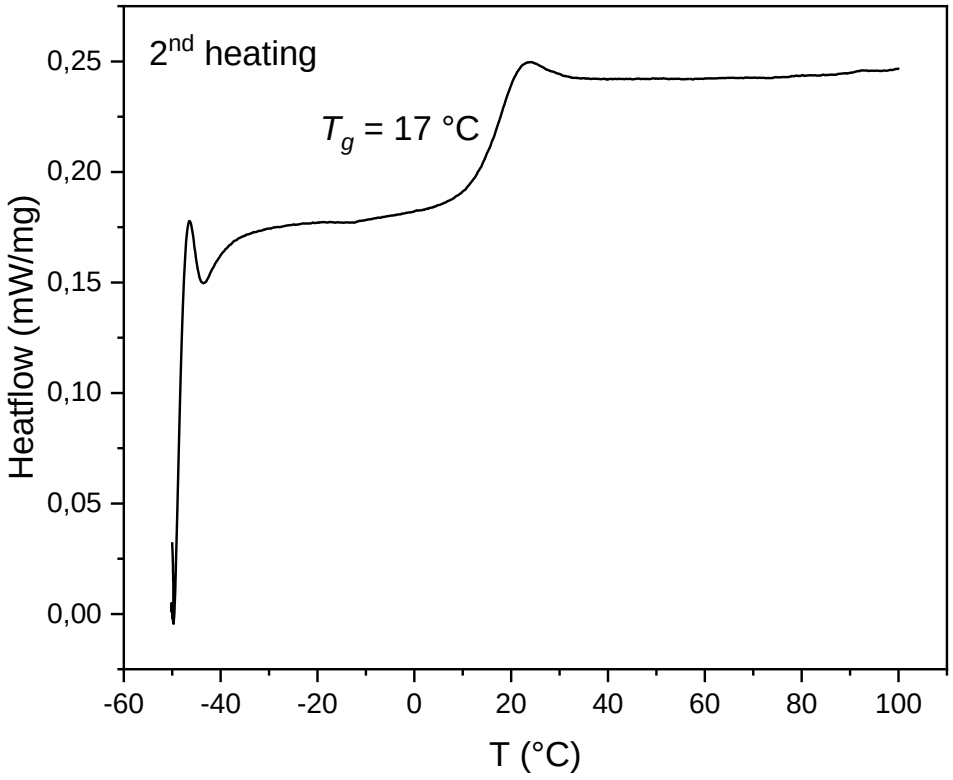

Figure S 61: DSC heating curve of the polymer corresponding table 2, run #4.

Section S5: Tetrapolymerisation

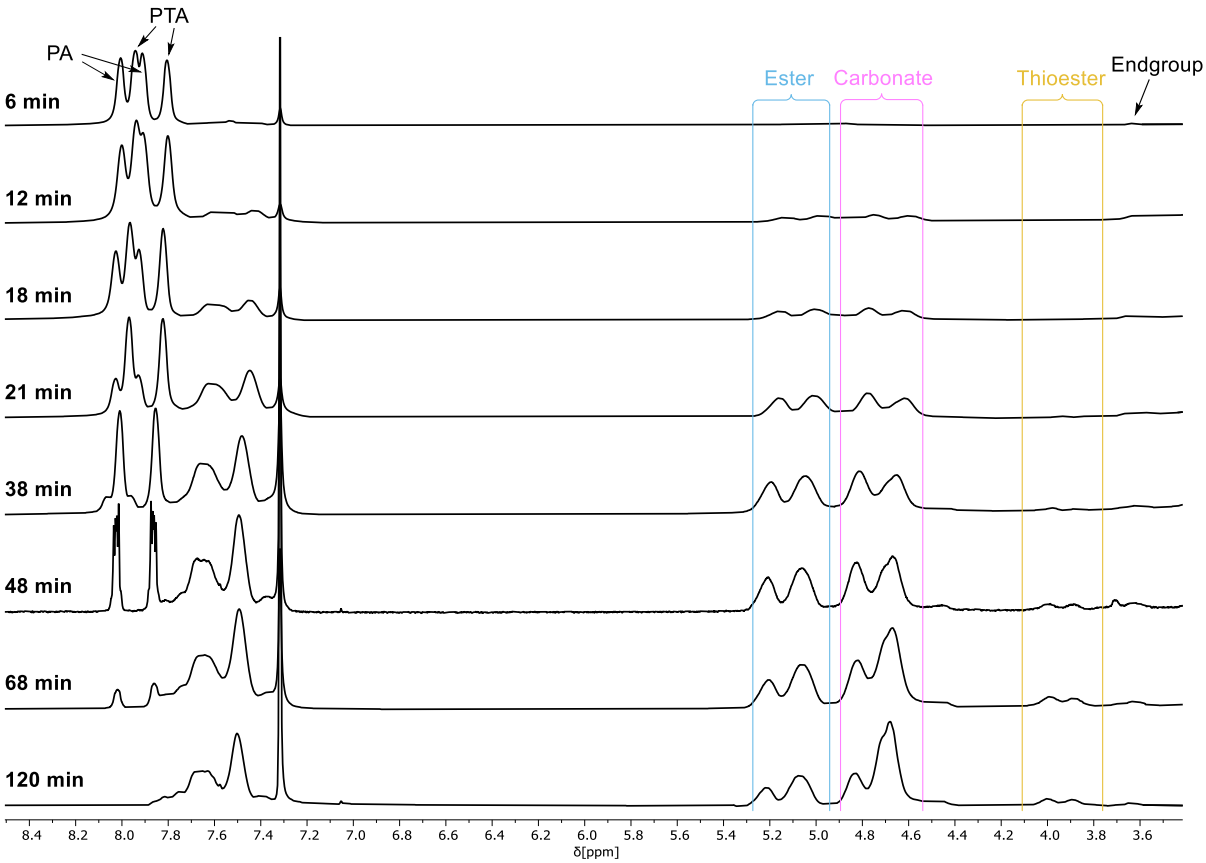

Figure S 62: Overlaid ^{1}H NMR spectra (400 MHz, $CDCl_3$, 25°C) of of the aliquots taken during tetrapolymerisation (1 eq. **L^{1}Cr^{K}**: 50 eq. PA: 50 eq. PTA: 1000 eq. CHO at 4 bar CO_2 pressure and 100°C) showing the consumption of PA before the consumption of PTA during polymerisation.

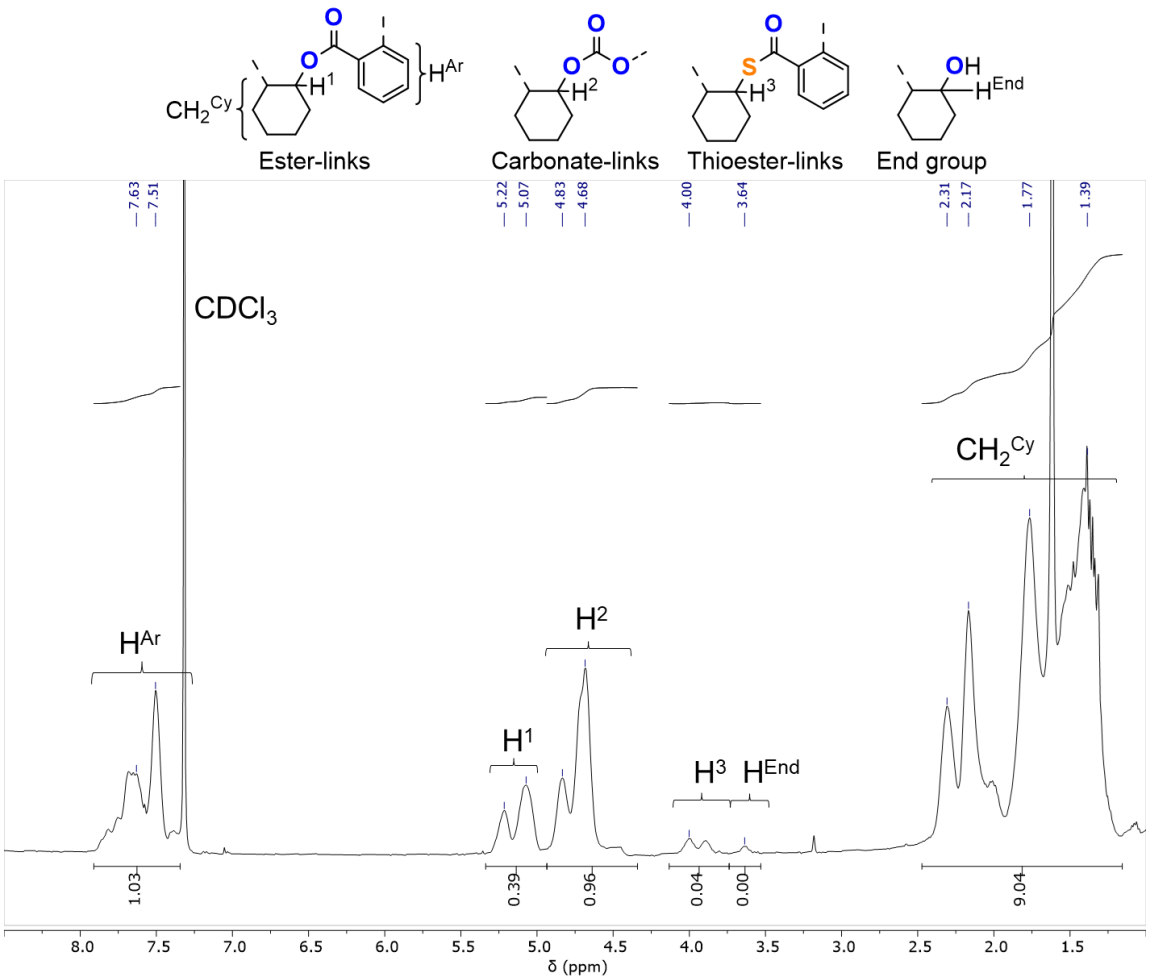

Figure S 63: ^{1}H NMR spectrum (400 MHz, $CDCl_3$, 25°C) of tetrapolymer isolated as outlined in the methods section.

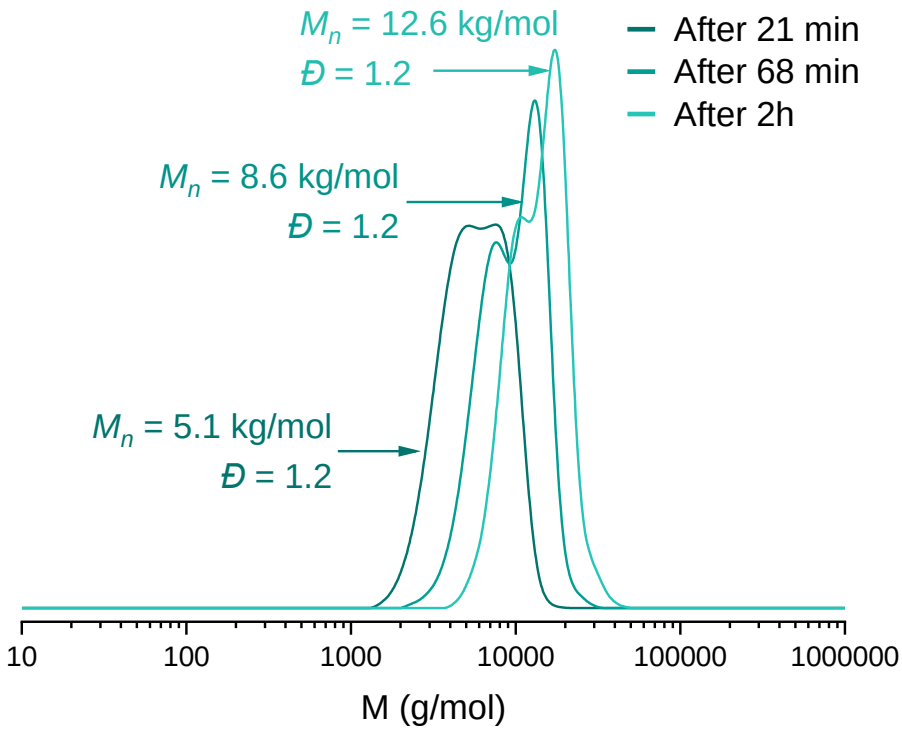

Figure S 64: Evolution of GPC traces with progress of tetrapolymerisation.

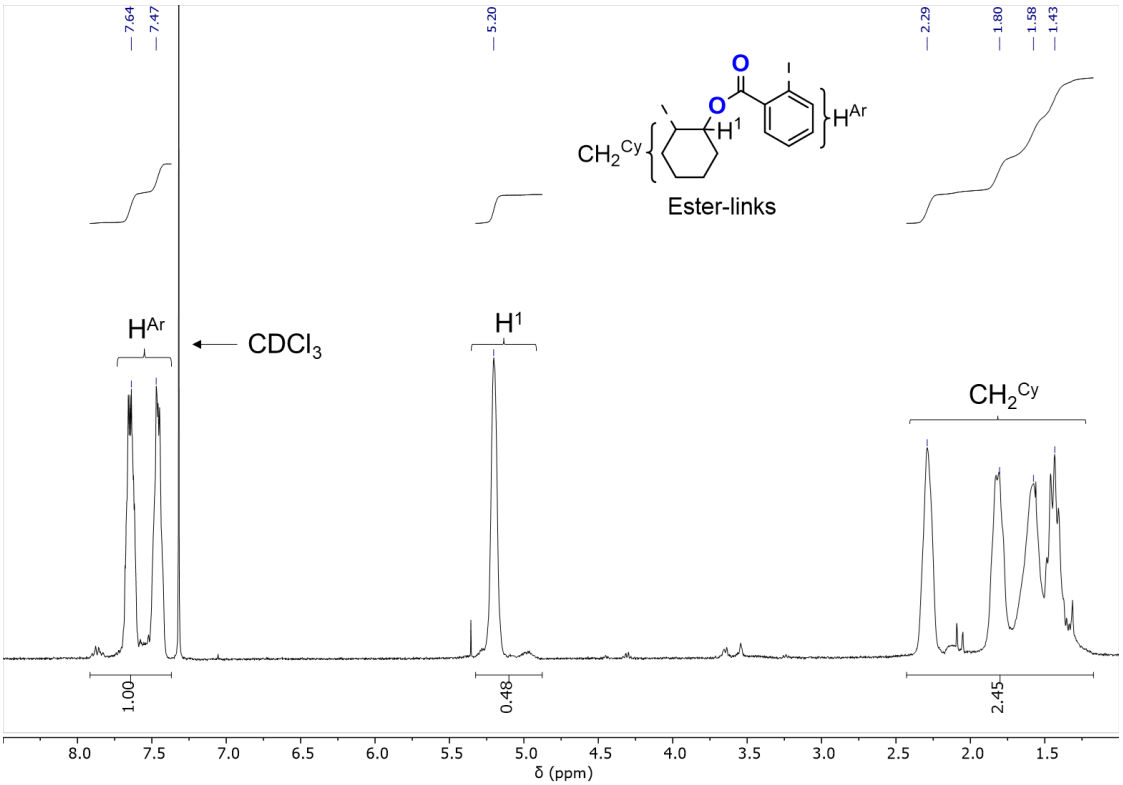

Figure S 65: ^{1}H NMR spectrum (25°C, $CDCl_3$) of the copolymer obtained from PA/CHO ROCOP.

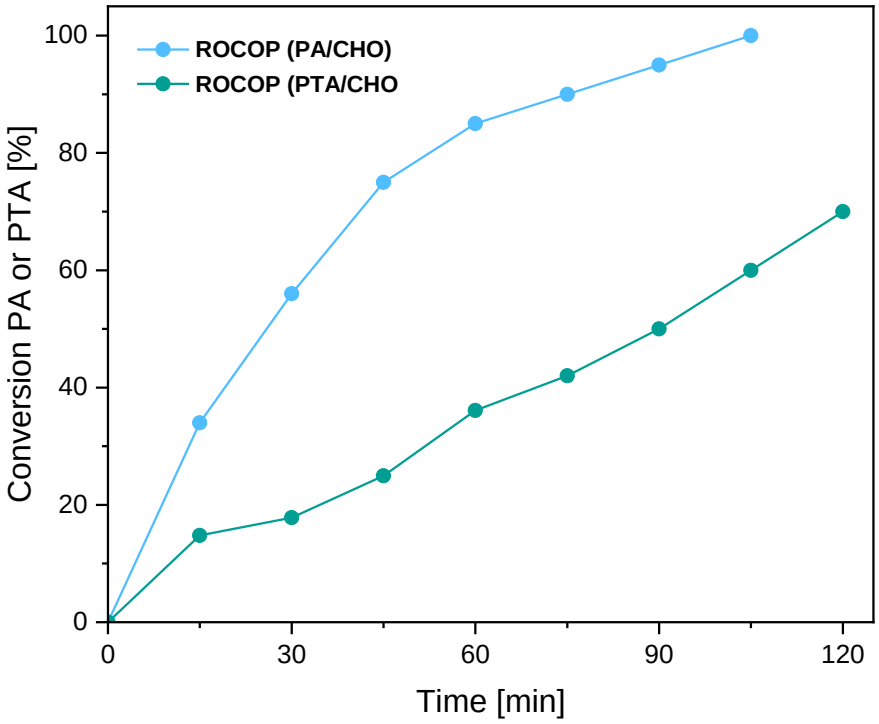

Figure S 66: Conversion of PA or PTA *versus* time plot for PA/CHO and PTA/CHO ROCOP. Initial TOF for PA/CHO ROCOP was determined between 0 and 45 min.

Section S6: Degradation studies

UV degradation: The respective polymer (50 mg) was dissolved in $CDCl_3$ (0.75 mL) and irradiated for 14h by a broadband Hg UV 1000W UV lamp inside a J. Young NMR tube. Afterwards the sample was analysed by ^1H NMR spectroscopy and GPC.

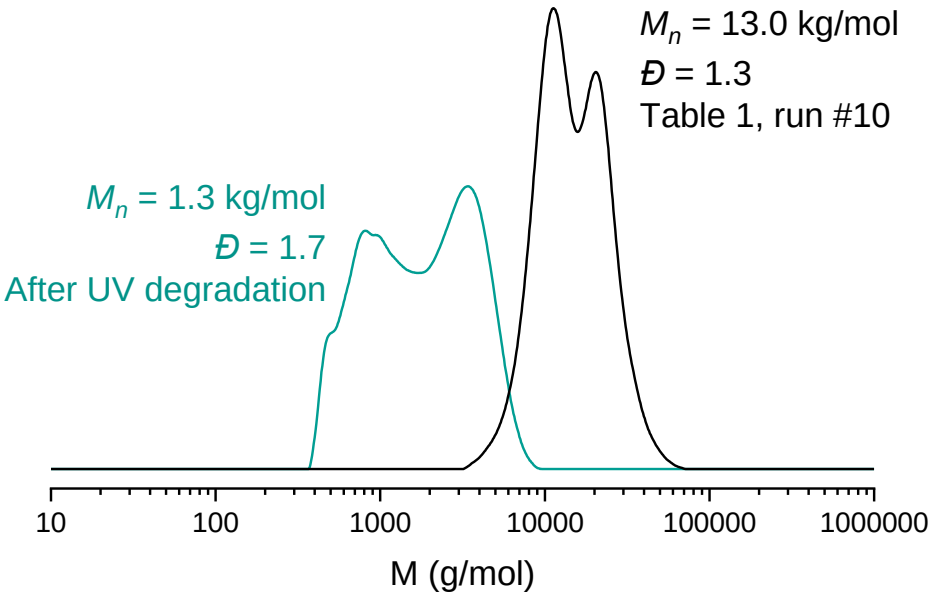

Figure S 67: SEC traces of the terpolymer corresponding to table 1, run #10 before and after irradiation showing complete degradation into oligomers under UV light in $CDCl_3$.

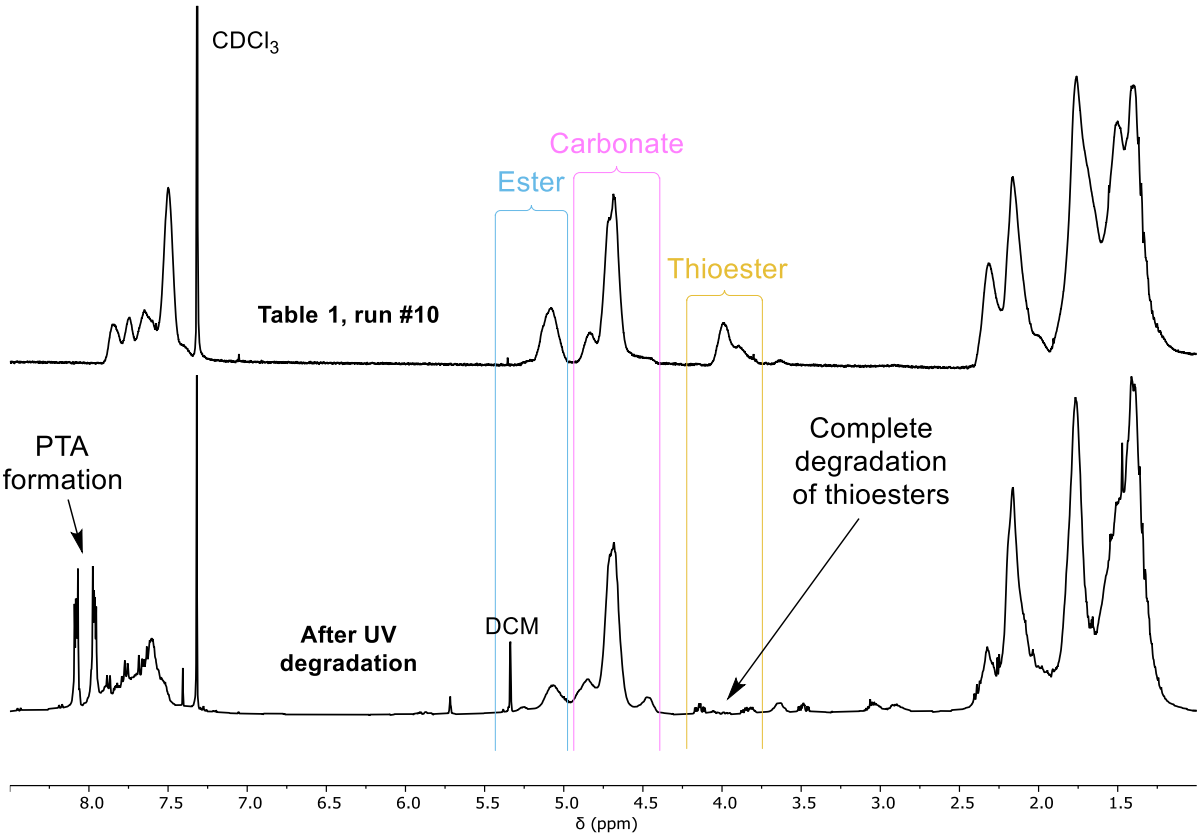

Figure S 68: Overlaid ^{1}H NMR spectra (400 MHz, CDCl3, 25°C) of the terpolymer corresponding to table 1, run #10 before and after irradiation showing complete degradation of thioesters under UV light in $CDCl_3$ and identifying PTA as a major degradation product.

Aminolysis degradation: The respective polymer (50 mg) was suspended in 7 M ammonia in methanol (1 mL) in a 2 mL vial sealed with a melamine cap containing a Teflon inlay equipped with a flame dried magnetic stirrer for the specified time at room temperature.

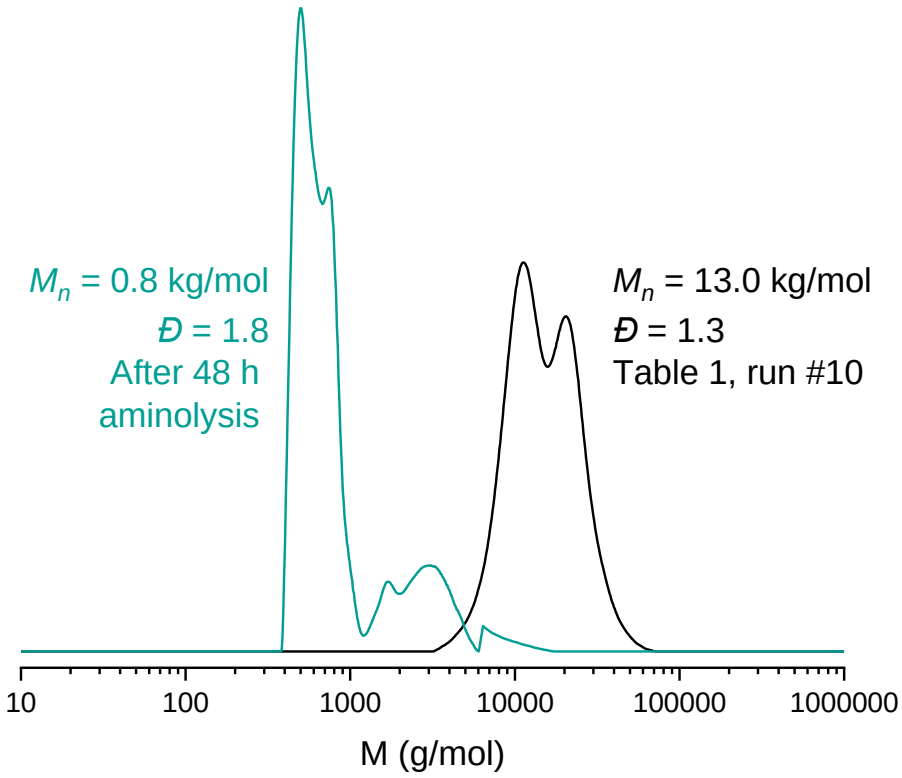

Figure S 69: GPC traces of the terpolymer corresponding to table 1, run #10 before and after aminolysis degradation showing complete degradation into oligomers.

A polycarbonate obtained from CHO/CO_2 ROCOP (M_n = 14.4 kg/mol and Đ = 1.5, see Ref. [7]) as well as a polyester obtained from CHO/PA ROCOP (M_n = 16.9 kg/mol and Đ = 1.3) using **L^1Cr^{Cs}** as catalyst were used in a comparative aminolysis degradation experiment under identical conditions and reaction times. Both copolymers showed no change in molecular weight within 48 hours and thus no evidence of degradation.

Section S7: Crystallography

X-Ray data were collected on a BRUKER D8 Venture system. Data were collected at 100(2) K using graphite-monochromated Mo K_α radiation (λ_α = 0.71073 Å). The strategy for the data collection was evaluated by using the Smart software. The data were collected by the standard "*ψ*-*ω* scan techniques" and were scaled and reduced using Saint+software. The structures were solved by using Olex2,[9] the structure was solved with the XT[10] structure solution program using Intrinsic Phasing and refined with the XL refinement package[11,12] using Least Squares minimization. If it is noted, bond length and angles were measured with Diamond Crystal and Molecular Structure Visualization Version 4.6.2.[13] Drawings were generated with POV-Ray.[14]

Compound	**L^2Cr**
Empirical formula	$C_{25}H_{27}CrN_2O_8$
Formula weight	535.48
Temperature/K	100.0
Crystal system	triclinic
Space group	P-1
a/Å	10.7338(8)
b/Å	10.8127(8)
c/Å	11.6585(9)
α/°	98.341(3)
β/°	100.448(3)
γ/°	115.303(3)
Volume/Å^3	1164.70(15)
Z	2
ρ_{calc}g/cm^3	1.527
μ/mm^{-1}	0.547
F(000)	558.0
Crystal size/mm^3	0.9 × 0.8 × 0.11
Crystal shape	Block
Crystal color	red
Radiation	MoKα (λ = 0.71073)
2Θ range for data collection/°	4.304 to 50.898
Index ranges	-12 ≤ h ≤ 12, -13 ≤ k ≤ 13, -14 ≤ l ≤ 14
Reflections collected	38482
Independent reflections	4276 [R_{int} = 0.0672, R_{sigma} = 0.0353]
Data/restraints/parameters	4276/0/338
Goodness-of-fit on F^2	1.042
Final R indexes [I>=2σ (I)]	R_1 = 0.0506, wR_2 = 0.1328
Final R indexes [all data]	R_1 = 0.0607, wR_2 = 0.1391
Largest diff. peak/hole / e Å^{-3}	0.77/-0.68

Section S8: Bibliography

[1] W. Feng, Y. Zhang, X. Lü, Y. Hui, G. Shi, D. Zou, J. Song, D. Fan, W.-K. Wong, R. A. Jones, *CrystEngComm* **2012**, *14*, 3456–3463.

[2] W.-K. Lo, W.-K. Wong, W.-Y. Wong, J. Guo, K.-T. Yeung, Y.-K. Cheng, X. Yang, R. A. Jones, *Inorg. Chem.* **2006**, *45*, 9315–9325.

[3] E. F. Reid, V. C. Cook, D. J. D. Wilson, C. F. Hogan, *Chem. Eur. J.* **2013**, *19*, 15907–15917.

[4] A. A. Abdel Aziz, H. A. Elbadawy, *Spectrochim. Acta Part A* **2014**, *124*, 404–415.

[5] S. Majumder, R. Koner, P. Lemoine, M. Nayak, M. Ghosh, S. Hazra, C. R. Lucas, S. Mohanta, *Eur. J. Inorg. Chem.* **2009**, *2009*, 3447–3457.

[6] A. Thevenon, J. A. Garden, A. J. P. White, C. K. Williams, *Inorg. Chem.* **2015**, *54*, 11906–11915.

[7] J. Stephan, M. R. Stühler, S. M. Rupf, S. Neale, A. J. Plajer, *Cell Rep. Phys. Sci.* **2023**, *101510*.

[8] L.-Y. Wang, G.-G. Gu, T.-J. Yue, W.-M. Ren, X.-B. Lu, *Macromolecules* **2019**, *52*, 2439-2445.

[9] O. V. Dolomanov, L. J. Bourhis, R. J. Gildea, J. A. K. Howard, H. Puschmann, *J. Appl. Cryst.* **2009**, *42*, 339–341.

[10] G. M. Sheldrick, *Acta Cryst.* **2015**, *A71*, 3–8.

[11] G. M. Sheldrick, *SHELXL Version 2014/7, Program for Chrystal Structure Solution and Refinement*, Göttingen, Germany, **2014**.

[12] G. M. Sheldrick, *Acta Cryst.* **2008**, *A64*, 112–122.

[13] K. Brandenburg, “Diamond: Crystal and Molecular Structure Visualization,” can be found under http://www.crystalimpact.com/diamond, **2017**.

[14] Persistance of Version Pty. Ltd., **2004**, Retrieved from http://www.povray.org/download/.